 ©2009 Kvantovaya Elektronika and Turpion Ltd

REVIEW

PACS numbers: 42.55.Ks; 33.50.–j; 82.20.–w
DOI: 10.1070/QE2009v039n11ABEH014014

Excited states in the active media of oxygen–iodine lasers

V.N. Azyazov

Contents

1. Introduction 989
2. Features of kinetic processes in the active medium of a chemical oxygen–iodine laser 990
   2.1. Detection of vibrationally excited O_2 molecules
   2.2. Production and relaxation of $I_2(v)$
   2.3. Kinetics of electronically excited $I_2(A', A, B)$ molecules
   2.4. Dissociation channels of I_2 in the active medium of an oxygen–iodine laser
3. Excitation and deactivation kinetics of O_2(a) and I^* in the active media of electric-discharge and photolysis oxygen–iodine lasers 998
   3.1. Quenching of O_2(a) in the $O(^3P) - O_2(X) - O_2(a)$ mixture
   3.2. Quantum yield of O_2(a) in reactions of $O(^1D)$ with N_2O and of $O(^3P, ^1D)$ with NO_2
   3.3. Quenching of I^* by $O(^3P)$, O_3, NO_2, N_2O_4, and N_2O molecules
4. Conclusions 1004
5. References 1004

Abstract. **A review of investigations of kinetic processes in active media oxygen–iodine lasers (OILs) performed in the last decade is presented. The mechanisms of pumping and quenching of electronically and vibrationally excited O_2 and I_2 molecules are considered, and dissociation mechanisms of I_2 in the active medium of the OIL are analysed. The values of kinetic constants of processes proceeding in the active media of OILs are recommended.**

Keywords*: oxygen–iodine laser, singlet oxygen, dissociation of I_2, vibrationally excited oxygen, $I(^2P_{1/2})$, $O(^3P)$, $O(^1D)$, $O_2(a\,^1\Delta_g)$, $O_2(b\,^1\Sigma_g^+)$, $I_2(A', A)$, $I_2(B)$, N_2O, NO_2, N_2O_4, O_3.*

1. Introduction

Laser systems operating on atomic iodine are classified by the method of excitation of the electronic $I(^2P_{1/2}) \rightarrow I(^2P_{3/2})$ transition. The population inversion at the $I^* \rightarrow I$ transition has been achieved by different methods: the photodissociation of iodine-containing molecules, the electron-impact dissociation of alkyl iodide molecules, and the electronic energy transfer from the metastable states of molecules. In 1964 Kasper and Pimentel [1] obtained for the first time the population inversion at the $I^* \rightarrow I$ transition in the pulsed UV photolysis of alkyl- and perfluoralkyl iodides CX_3I (X = H, F). The quantum yield of excited I^* atoms in the UV photolysis of some iodides exceeds 90 % [2–4], which stimulated the rapid development of a photodissociation iodine laser. The kinetics of primary and secondary processes in the active medium of this laser has been studied in many papers. The sets of recommended kinetic constants are presented in [5–7]. [Below, the following notations are used: I, I^* are iodine atoms in the states $^2P_{3/2}$ and $^2P_{1/2}$ ($E = 7603$ cm^{-1}); O_2(X), O_2(a), O_2(b) are oxygen molecules in the electronic states $X\,^3\Sigma_g^-$, $a\,^1\Delta_g$ (7882 cm^{-1}), $b\,^1\Sigma_g^+$ (13121 cm^{-1}); and I_2(X), $I_2(A')$, $I_2$2(A), I_2(B) are iodine molecules in the states $X\,^1\Sigma_g^+$, $A'\,^3\Pi_{2u}$ (10047 cm^{-1}), $A\,^3\Pi_{1u}$ (10847 cm^{-1}), $B\,^3\Pi_0$ (15725 cm^{-1}).]

The method of production of I^* atoms by the electron-impact dissociation of alkyl iodide molecules has not found wide applications first of all because the quantum yield of I^* in this process is about 50 % [5]. In addition, the production of a stable discharge in media containing alkyl iodides proved to be a complicated problem.

The $I^* \rightarrow I$ spin–orbit transition in atomic iodine can be also inverted by transferring energy to I atoms from metastable electronically excited molecules or atoms. The attempts to obtain lasing at the $I^* \rightarrow I$ transition inverted due to energy transfer have been successful only for two donor molecules $O_2(a\,^1\Delta)$ [8] and NCl ($a\,^1\Delta$) [9, 10]. These molecules have metastable singlet states and their transition to the ground $X\,^3\Sigma$ state is forbidden by the selection rules. The rates of collision deactivation of these molecules are relatively small, especially for a homonuclear oxygen molecule. However, they efficiently transfer their excitation energy to atomic iodine in processes

V.N. Azyazov Samara Branch, P.N. Lebedev Physics Institute, Russian Academy of Sciences, ul. Novo-Sadovaya 221, 443011 Samara, Russia; e-mail: azyazov@fian.smr.ru

Received 28 November 2008; revision received 3 July 2009
Kvantovaya Elektronika **39** (11) 989–1007 (2009)
Translated by M.N. Sapozhnikov

$$O_2(a\,^1\Delta) + I \leftrightarrow O_2(X\,^3\Sigma) + I^* + 280\ cm^{-1}, \quad (i)$$

$$NCl(a\,^1\Delta, v = 0) + I \rightarrow NCl(X\,^3\Sigma, v = 2) + I^* + 50\ cm^{-1} \quad (ii)$$

with the rate constants $K_i = 7.8 \times 10^{-11}$ cm^3 s^{-1} [11] and $K_{ii} = 2 \times 10^{-11}$ cm^3 s^{-1} [12, 13] (v is the vibrational quantum number). The use of process (ii) to obtain inversion at the laser transition proved to be complicated mainly due to the complexity and low efficiency of generators of electronically excited $NCl(a\,^1\Delta)$ molecules.

One of the promising methods of inverting the $I^* \rightarrow I$ laser transition is energy transfer to atomic iodine from the metastable electronic state of $O_2(a)$ [process (i)]. The equilibrium constant of reaction (i) $K_{eq} = K_i^+/K_i^- = 0.75\exp(402/T)$ [14] determines the threshold relative content $\eta_\Delta = [O_2(a)]/[O_2]$ of electronically excited singlet oxygen molecules above which a gas medium containing singlet oxygen and iodine can amplify light: $\eta_\Delta^{th} = (1 + 2K_{eq})^{-1}$. Here, K_i^+ and K_i^- are the rate constants of reaction (i) in the forward and backward directions, respectively; $[O_2] = [O_2(a)] + [O_2(X)]$; $[O_2(X)]$ and $[O_2(a)]$ are the oxygen concentrations in the ground and singlet electronic states, respectively. The threshold content of $O_2(a)$ at the gas mixture temperature $T = 300$ K is 15 %. Dramatic progress in the development of oxygen–iodine lasers (OILs) has been achieved first of all due to the existence of highly efficient singlet-oxygen generators (SOGs). Singlet oxygen can be produced by numerous methods [15, 16]. We consider only photolysis, electric-discharge, and chemical methods that are used in operating OILs. Depending on the type of a generator used in the laser, there exist a photolysis OIL (POIL), an electric-discharge OIL (EOIL) and a chemical OIL (COIL).

The greatest progress has been achieved in the COIL development, where $O_2(a)$ is produced during chlorination of an alkali solution of hydrogen peroxide. However, there also exist other promising directions in the development of OILs, which cannot be realised in the COIL. In particular, it is quite difficult to organise a closed cycle in the COIL scheme. The exhaust of waste gases to the atmosphere is accompanied by a considerable energy consumption, which reduces the total efficiency of the system. Toxic reagents (Cl_2, I_2, KOH) make the COIL unattractive for wide applications.

At present EOILs, in which $O_2(a)$ is produced in plasma-chemical processes, attract great interest. The realisation of a closed cycle in the EOIL appears feasible. It is assumed that oxygen and buffer gas circulate continuously in a closed loop, while molecular iodine and heat are selected in a trap and a heat exchanger, respectively. A low pressure of O_2 at the output of an electric-discharge SOG (up to 10 Torr) and a low relative content of excited singlet oxygen molecules ($\eta_\Delta \approx 15\,\% - 20\,\%$) do not allow the EOIL to compete successfully with the COIL so far.

Investigations of the kinetics of the active media of OILs performed for many years have led to the development of a megawatt cw laser [17]. However, the potential of OILs is far from being exhausted. Recent studies of the kinetics of the excited states of particles in the active medium of OILs open up new directions of their further development. Interest in the studies of excited states in oxygen-containing media is also caused by the demands of atmospheric physics [18, 19], laser physics [20], plasma physics [21, 22], combustion and explosion physics [23], biology [24], and medicine [25].

The kinetics of processes in the OIL media has been studied in many theoretical and experimental papers [11, 14, 21, 22, 26–84]. Because the COIL was for a long time a favourite among other types of OILs, the kinetics of chemical lasers was investigated most thoroughly. The rate constants of processes in the active medium of COILs and methods of their measurement were analysed in [54]. The most complete kinetic scheme of processes in the medium of a chemical laser is presented in [11]. This scheme, which is called the standard kinetic package (SKP) for a COIL, was used for simulations of the kinetics of laser media for more than ten years. During this time, new kinetic data were obtained which considerably changed the concepts of some mechanisms of excitation and deactivation of excited states in the COIL medium. Numerous kinetic data about processes proceeding in the active media of POIL and EOIL were also accumulated. The present review considers new kinetic data and analyses the mechanisms of pumping and quenching of electronically and vibrationally excited states in oxygen-iodine media.

2. Features of kinetic processes in the active medium of a chemical oxygen–iodine laser

Inversion produced at the $I^* \rightarrow I$ laser transition during electronic energy transfer from singlet oxygen to atomic iodine was first obtained by using a chemical SOG in which $O_2(a)$ was generated in the interaction of $ClSO_3F$ with the alkali solution of hydrogen peroxide [43]. The first OIL emitting 4 mW had a gas–liquid generator in which gaseous Cl_2 was bubbled through a $H_2O - H_2O_2 - NaOH$ solution layer [8]. The generation of $O_2(a)$ by chlorination of the alkali solution of hydrogen peroxide proved to be the most efficient and is now used in most operating OILs.

During the contact of the solution surface with gas, Cl_2 molecules penetrate through the interface into the solution, where they react with HO_2^- ions in a narrow surface layer:

$$Cl_2 + HO_2^- \rightarrow HCl + Cl^- + O_2(a).$$

The $O_2(a)$ yield in this reaction is close to 100 % [44, 45, 85, 86]. The rate constant of the liquid–phase reaction was most reliably measured in a reactor with a single laminar jet [42]. $O_2(a)$ produced in the liquid diffuses to the surface and is desorbed to the gas phase. To produce efficiently oxygen in the excited electronic state, first, the residence time of $O_2(a)$ in the solution should be much shorter than its lifetime in the solution, which is equal to 2×10^{-6} s [15, 87] and, second, chlorine should be utilised for the time shorter than the $O_2(a)$ quenching time in the gas-phase pooling reaction $O_2(a) + O_2(a) \rightarrow O_2(b) + O_2(X)$.

These two conditions of the efficient operation of a chemical SOG can be realised in a number of gas–liquid devices widely used in chemical technology. In the first OILs, a bubbling SOG was mainly used [8, 88–91] because of its simplicity and rather high efficiency. The high relative content of excited oxygen ($\eta_\Delta \geqslant 0.5$) at the output of this generator is preserved down to pressures of a few torr. In film gas–liquid generators, gas and liquid come in contact on the liquid-wetted surface (attachment surface) representing tubes or plates [92]. By using a disk film $O_2(a)$ generator, a 35-kW COIL was developed [93].

One of the urgent problems to be solved for the development of high-power pulsed and cw OILs is the construction of high-pressure $O_2(a)$ generators. In the case of pulsed OILs, this will provide an increase in the specific energy extraction from the active medium volume [94–96]. For cw OILs with the supersonic flow of the active medium, an increase in the initial oxygen pressure leads to the increase in the Mach number by preserving the high density of $O_2(a)$ in the resonator and also simplifies a system for waste gas exhaust to the atmosphere [47, 97]. Oxygen–iodine lasers based on a high-pressure SOG do not require water vapour traps [98, 99]. A jet SOG allows the production of $O_2(a)$ at the concentration up to 10^{18} cm^{-3} and the singlet oxygen yield above 50 % [100]. Based on a jet SOG, a 12-kW OIL was built [101].

Recently, by using a gas–liquid generator combining the properties of jet, aerosol, and disk generators, a 50-kW COIL was developed [102]. Based on a jet-drop SOG, a megawatt COIL was developed [17]. Quite recently [103, 104], a SOG with a rotating bubbling layer with the centrifugal acceleration of about $400g$ was tested. This generator has two important advantages: a high (1.34 mmol s^{-1}) specific chlorine flow rate per unit area over the bubbling layer and a low (3.7 cm^3 mmol^{-1}) volume flow rate of solution per unit flow rate of molecular chlorine.

In pulsed OILs, atomic iodine is generated by using the dissociation of perfluoralkyl iodides caused by UV radiation [51, 94–96] or an electric discharge [105]. In cw OILs, I_2 vapours are predominantly used, which are added to an oxygen-containing gas flow [8]. Molecular iodine rapidly dissociates interacting with $O_2(a)$ [26–29]. This method is attractive because it does not require the consumption of external energy. The dissociation efficiency of I_2 in an OIL is usually empirically defined as the number of $O_2(a)$ molecules spent for dissociation of one I_2 molecule. This parameter is not constant and depends on experimental conditions, mainly because the dissociation process includes several stages. The influence of dissociation on the energy efficiency of OILs was demonstrated in recent papers [52, 106]. In [106], the energy efficiency of the laser was increased from 33 % to 40 % by reducing the number of $O_2(a)$ molecules spent for dissociation of one I_2 molecule. In experiments [106], 4.2 $O_2(a)$ molecules were spent for dissociation of one iodine molecule.

Depending on the design of a mixing unit, from 4 to 16 $O_2(a)$ molecules can be spent for dissociation of one I_2 molecule [52, 107]. To avoid $O_2(a)$ losses for dissociation of iodine, the OIL schemes with the external production of iodine atoms by chemical [108] or electric-discharge [109–113] methods were considered. However, so far the OIL schemes with the external production of iodine atoms have not led to a noticeable improvement in the output parameters of OILs.

The rate constants of elementary processes presented in the SKP [11] were measured accurately enough, except the rate constants of processes responsible for dissociation of I_2 (processes from the SKP are presented in Table 1 in regular font). The key process in OILs of all types is the electronic energy exchange between O_2 and I [processes (40) and (41)]. (All reactions considered is section 2 and their rate constants are presented in Table 1.) The rate constant of process (41) was measured by different methods in papers [56–61, 114]. The rate constant K_{40} is related to K_{41} by the expression $K_{40} = 0.75K_{41}\exp(402/T)$ [14]. The temperature dependence of the rate constant of energy transfer from I^* to $O_2(X)$ was studied in [56] by the method of laser photolysis of the $O_2 - I_2$ mixture at a wavelength of 498 nm. The gas flow was cooled during its adiabatic expansion in a supersonic nozzle.

The rate constants of the excitation and deactivation of the excited electronic states of $O_2(a)$, $O_2(b)$, and I^* were

Table 1. Kinetic processes in the active medium of a COIL and their rate constants.

Reaction number	Reaction	Rate constant* ($T = 300$ K)
1	$O_2(a) + O_2(a) \rightarrow O_2(b, v) + O_2(X)^{**}$	2.5×10^{-17}
2	$O_2(a) + O_2(a) \rightarrow O_2(a) + O_2(X)$	0
3	$O_2(a) + O_2(a) \rightarrow 2O_2(X, v)$	1.7×10^{-17}
4	$O_2(b) + O_2(X) \rightarrow O_2(a) + O_2(X)$	3.9×10^{-17}
5	$O_2(b) + H_2O \rightarrow O_2(a, v) + H_2O$	6.7×10^{-12}
6	$O_2(b) + Cl_2 \rightarrow O_2(a) + Cl_2$	2.0×10^{-15}
7	$O_2(b) + H_2O_2 \rightarrow O_2(a) + H_2O_2$	3.3×10^{-13}
8	$O_2(b) + He \rightarrow O_2(a) + He$	1.0×10^{-17}
9	$\mathbf{O_2(b) + CO_2 \rightarrow O_2(a, v) + CO_2^{***}}$	6.0×10^{-13}
14	$O_2(a) + O_2(X) \rightarrow O_2(X) + O_2(X)$	1.6×10^{-18}
15	$O_2(a) + H_2O \rightarrow O_2(X) + H_2O$	4.0×10^{-18}
16	$O_2(a) + Cl_2 \rightarrow O_2(X) + Cl_2$	6.0×10^{-18}
17	$O_2(a) + H_2O_2 \rightarrow O_2(X) + H_2O_2$	0
18	$O_2(a) + He \rightarrow O_2(X) + He$	8.0×10^{-21}
21	$I_2(X) + O_2(b) \rightarrow I + I + O_2(X)$	3.5×10^{-11}
22	$I_2(X) + O_2(b) \rightarrow I_2(X) + O_2(a)$	2.3×10^{-11}
24	$I_2(X) + O_2(b) \rightarrow I_2(A, A') + O_2(X)$	0
25	$I_2(A, A') + O_2(a) \rightarrow I + I + O_2(X)$	3.0×10^{-11}
26	$I_2(A, A') + O_2(a) \rightarrow I_2(B) + O_2(X)$	$< 10^{-12}$
27	$I_2(B) + M \rightarrow I + I + M$	6.0×10^{-11} (M = O_2)
28	$\mathbf{I_2(A') + O_2(X) \rightarrow I_2(X) + O_2(a)}$	6.3×10^{-12}
29.1	$\mathbf{I_2(A') + H_2O \rightarrow I_2 + H_2O}$	3.4×10^{-12}
29.2	$\mathbf{I_2(A') + N_2 \rightarrow 2I + N_2}$	3.5×10^{-14}
29.3	$\mathbf{I_2(A') + CO_2 \rightarrow I_2 + CO_2}$	8.5×10^{-13}
29.4	$\mathbf{I_2(A') + He \rightarrow 2I + He}$	9.4×10^{-15}
30	$I_2(B) \rightarrow I + I$	6.0×10^5 s^{-1}
31	$I_2(B) \rightarrow I_2(X) + h\nu$	6.0×10^5 s^{-1}
32	$I_2(X) + O_2(a) \rightarrow I_2(X, v) + O_2(X)$	$< 5.0 \times 10^{-16}$
33	$I_2(X) + I^* \rightarrow I_2(X, v > 10) + I$	3.8×10^{-11}
34	$I_2(X, \geqslant 25) + O_2(a) \rightarrow I + I + O_2(X)$	3.0×10^{-10}
35	$\mathbf{I_2(X, v) + O_2 \rightarrow I_2(X, v - 1) + O_2}$	$v \times 2.7 \times 10^{-12}$
36	$\mathbf{I_2(X, v) + H_2O \rightarrow I_2(X, v - 1) + H_2O}$	$v \times 6.0 \times 10^{-12}$
37	$\mathbf{I_2(X, v) + He \rightarrow I_2(X, v - 1) + He}$	$v \times 3.9 \times 10^{-12}$
38	$\mathbf{I_2(X, v) + N_2 \rightarrow I_2(X, v - 1) + N_2}$	$v \times 3.4 \times 10^{-12}$
39	$\mathbf{I_2(X, v) + CO_2 \rightarrow I_2(X, v - 1) + CO_2}$	$v \times 6.0 \times 10^{-12}$
40	$I + O_2(a) \rightarrow I^* + O_2(X)$	7.8×10^{-11}
41	$I^* + O_2(X) \rightarrow I + O_2(a)$	2.7×10^{-11}
42	$I + O_2(a) \rightarrow I + O_2(X)$	1.0×10^{-15}
43	$I^* + O_2(X) \rightarrow I + O_2(X)$	0
44	$I^* + O_2(a) \rightarrow I + O_2(b, v)$	1.1×10^{-13}
45	$I^* + O_2(a) \rightarrow I + O_2(a, v)$	1.1×10^{-13}
46	$I^* + O_2(a) \rightarrow I + O_2(X)$	0
47	$I^* + I \rightarrow I + I$	1.6×10^{-14}
48	$I^* + H_2O \rightarrow I + H_2O$	2.0×10^{-12}
49	$I^* + H_2O_2 \rightarrow I + H_2O_2$	2.5×10^{-11}
50	$I^* + He \rightarrow I + He$	5.0×10^{-18}
51	$I^* + O_2(X) \rightarrow I + O_2(X)$	3.5×10^{-16}
53	$I^* \rightarrow I + h\nu$	7.8 c^{-1}
54	$I^* + Cl_2 \rightarrow ICl + Cl$	5.5×10^{-15}

Continued on the next page

Continuation of Table 1.

56	$I^* + ICl \rightarrow I_2 + Cl$	1.5×10^{-11}
57	$I_2 + Cl \rightarrow ICl + I$	2.0×10^{-10}
58	$ICl + Cl \rightarrow Cl_2 + I$	8.0×10^{-12}
59	$I + I + I_2(X) \rightarrow I_2(X) + I_2(X)$	3.6×10^{-30} cm^6 s^{-1}
60	$I^* + I + I_2(X) \rightarrow I_2(B) + I_2(X)$	$< 3.6 \times 10^{-30}$ cm^6 s^{-1}
61	$I + I + He \rightarrow I_2(X) + He$	3.6×10^{-33} cm^6 s^{-1}
62	$I + I + O_2(X) \rightarrow I_2(X) + O_2(X)$	3.7×10^{-32} cm^6 s^{-1}
63	$I^* + I + M \rightarrow I_2(B) + M$	–
70	$\mathbf{O_2(\upsilon) + O_2 \rightarrow O_2(\upsilon - 1) + O_2}$	8.2×10^{-19}
71	$\mathbf{O_2(\upsilon) + H_2O \rightarrow O_2(\upsilon - 1) + H_2O}$	8.2×10^{-17}
72	$\mathbf{O_2(\upsilon) + He \rightarrow O_2(\upsilon - 1) + He}$	0
73	$\mathbf{O_2(\upsilon) + N_2 \rightarrow O_2(\upsilon - 1) + N_2}$	0
76	$\mathbf{O_2(X, 2) + O_2(X, 0) \rightarrow O_2(X, 1) + O_2(X, 1)}$	2.0×10^{-13}
77	$\mathbf{O_2(X, 3) + O_2(X, 0) \rightarrow O_2(X, 2) + O_2(X, 1)}$	2.6×10^{-13}
78	$\mathbf{O_2(X, 4) + O_2(X, 0) \rightarrow O_2(X, 3) + O_2(X, 1)}$	2.7×10^{-13}
79	$\mathbf{O_2(a, 1) + CO_2 \rightarrow O_2(a, 0) + CO_2(\upsilon)}$	1.8×10^{-14}
80	$\mathbf{O_2(a, 2) + CO_2 \rightarrow O_2(a, 1) + CO_2(\upsilon)}$	4.4×10^{-14}
81	$\mathbf{O_2(a, 3) + CO_2 \rightarrow O_2(a, 2) + CO_2(\upsilon)}$	1.0×10^{-13}
82	$\mathbf{O_2(b, 1) + CO_2 \rightarrow O_2(b, 0) + CO_2(\upsilon)}$	1.2×10^{-12}
83	$\mathbf{O_2(b, 2) + CO_2 \rightarrow O_2(b, 1) + CO_2(\upsilon)}$	1.7×10^{-12}
84	$\mathbf{O_2(b, 3) + CO_2 \rightarrow O_2(b, 2) + CO_2(\upsilon)}$	1.6×10^{-12}
85	$\mathbf{O_2(X, 1) + H_2(000) \rightarrow O_2(X, 0) + H_2O(010)}$	1.7×10^{-12}
89	$\mathbf{O_2(a, 1) + O_2(X, 0) \rightarrow O_2(X, 1) + O_2(a, 0)}$	5.6×10^{-11}
90	$\mathbf{O_2(a, 2) + O_2(X, 0) \rightarrow O_2(X, 2) + O_2(a, 0)}$	3.6×10^{-11}
91	$\mathbf{O_2(b, 1) + O_2(X, 0) \rightarrow O_2(X, 1) + O_2(b, 0)}$	1.52×10^{-11}
92	$\mathbf{O_2(b, 2) + O_2(X, 0) \rightarrow O_2(X, 2) + O_2(b, 0)}$	1.7×10^{-12}
93	$\mathbf{O_2(b, 3) + O_2(X, 0) \rightarrow O_2(X, 3) + O_2(b, 0)}$	1.5×10^{-13}
94	$\mathbf{H_2O(010) + H_2O \rightarrow H_2O(000) + H_2O}$	5.0×10^{-11}
95	$\mathbf{O_2(a, 1) + I_2(X) \rightarrow O_2(X) + I_2(A')}$	2.0×10^{-12}
96	$\mathbf{O_2(a, 2) + I_2(X) \rightarrow O_2(X) + I_2(A)}$	3.0×10^{-11}
97	$\mathbf{O_2(a, 3) + I_2(X) \rightarrow O_2(X) + 2I}$	1.0×10^{-11}
101	$\mathbf{O_2(a) + I_2(X, 11 \leqslant \upsilon \leqslant 24) \rightarrow O_2(X) + I_2(A')}$	$10^{-12} - 10^{-11}$
102	$\mathbf{O_2(a, 1) + I_2(X, \upsilon \geqslant 15) \rightarrow O_2(X) + 2I}$	1.0×10^{-11}
103	$\mathbf{O_2(a, 2) + I_2(X, \upsilon \geqslant 8) \rightarrow O_2(X) + 2I}$	1.0×10^{-11}

Notes: *If the dimensionality is not presented, the rate constant is measured in cm^3 s^{-1}; **processes from the SKP are presented in regular type [11]; ***processes supplementing the SKP are presented in bold type [124]; numbers in parentheses in processes (76)–(85) and (89)–(93) denote vibrational levels of O_2.

found with a high accuracy [56–63]. The rate constants of processes in the active medium of the COIL and their measurement methods were analysed in papers [11, 46, 54]. Processes involving O_2 in excited vibrational states are poorly studied and are not presented in the SKP [11]. This is explained first of all by the fact that the detection of $O_2(\upsilon)$ in the active medium of the OIL is a challenging problem because the oxygen molecule does no have the dipole moment.

2.1 Detection of vibrationally excited O_2 molecules

The deactivation of the electronic energy in EV processes (1), (5), (9), (33), (44), and (45) in the active medium of the OIL leads to the production of vibrationally excited O_2, H_2O, and I_2 molecules. In pooling reaction (1), vibrationally excited oxygen $O_2(b, \upsilon)$ is produced with the yield probabilities 0.32, 0.04, and 0.64 for $\upsilon = 0$, 1, and 2, respectively [115]. How the released energy is distributed among the products of pooling reaction (44) is unknown. The probability of producing vibrationally excited $H_2O(001)$ molecules in reaction (5) is 0.1 [116]. Calculations show that the greater part of energy released in reactions (1), (5), and (44) enters to the vibrational degrees of freedom of the products [116]. In reaction (48), vibrationally excited $H_2O(002)$ molecules are produced [117]. In [118–120], the formation of vibrationally excited iodine $I_2(X, 11 \leqslant \upsilon \leqslant 45)$ in reaction (33) was found. The vibrationally excited $I_2(\upsilon)$ and $O_2(\upsilon)$ molecules play an important role in the formation of the active medium of the COIL, especially during the dissociation of I_2.

The detection of $O_2(\upsilon)$ in the OIL medium was reported only in several papers. The emission of vibrationally excited $O_2(a, \upsilon = 1)$ and $O_2(b, \upsilon = 1)$ in the reaction zone of a bubbling SOG was observed in [121]. Lilenfeld [55] found the presence of $O_2(X, \upsilon)$ at the output of a chemical SOG by using EPR spectroscopy. However, the authors of these papers have failed to determine the $O_2(\upsilon)$ content quantitatively. The relative content of $O_2(a, \upsilon)$ was determined for the first time by comparing the intensities I_{634} and I_{579} of the luminescence bands of an oxygen dimole at 634 and 579 nm, respectively [122]:

$$O_2(a, \upsilon = 0) + O_2(a, \upsilon' = 0) \rightarrow O_2(X, \upsilon = 0) + O_2(X, \upsilon' = 0) + h\nu_{634},$$

$$O_2(a, \upsilon = 1) + O_2(a, \upsilon' = 0) \rightarrow O_2(X, \upsilon = 0) + O_2(X, \upsilon' = 0) + h\nu_{579}.$$

The emission band at 579 nm belongs to an oxygen dimole formed by two singlet oxygen molecules, one of which is vibrationally excited with $\upsilon = 1$. The rate R of emission of photons by the dimole is defined as the product of the rate constant by the concentration of oxygen molecules: $R_{579} = K_{579}[O_2(a, \upsilon = 0)][O_2(a, \upsilon = 1)]$ and $R_{634} = K_{634}[O_2(a, \upsilon = 0)][O_2(a, \upsilon = 0)]$. These rates are related to the emission intensities I_{579} and I_{634} by the expression $R_{579}/R_{634} = I_{579}/I_{634}$ [122]. After substitution of the experimental intensity ratio $I_{579}/I_{634} \approx 0.02$ [122] and the rate constant ratio $K_{579}/K_{634} = 0.93$ [123] into this expression, the relative vibrational population of singlet oxygen at the output of a jet–drop generator was found to be $[O_2(a, \upsilon = 1)]/[O_2(a, \upsilon = 0)] \simeq 0.02$ [122].

Vibrationally excited oxygen in the active medium of a COIL was detected in a low-pressure continuous-flow chamber by recording the luminescence spectra of O_2 molecules at vibronic transitions $O_2(b, \upsilon = i) \rightarrow O_2(X, \upsilon' = i) + h\nu_i$, where $i = 0$, 1 or 2 [77, 78, 80]. Singlet oxygen was generated in a jet SOG. The gas pressure P_g in the reaction zone of the SOG was ~ 35 Torr. Oxygen was supplied from the SOG to a measuring cell. Iodine vapour with a carrier gas (N_2) was injected into the oxygen flow at a distance of 16 cm from the SOG output. The gas pressure P_c in the measuring cell was ~ 3 Torr. Figure 1 presents the emission spectra of $O_2(b)$ in the wavelength range from 757 to 785 nm for two initial molecular fraction of iodine in the flow $\eta_{I_2} = G_{I_2}/G_{Cl_2}$ (G_{I_2} and G_{Cl_2} are the flow rates of I_2 and Cl_2, respectively). The observation point was located downstream at a distance of $L = 5$ cm from the iodine injection site [80]. The flow rates of chlorine and the buffer gas N_2 carrying I_2 vapours were the same: $G_{Cl_2} = G_{N_2} = 2.5$ mmol s^{-1}. The symbols R(bi–Xi) and P(bi–Xi) in Fig. 1 denote the contours of rotational R and P branches for three transitions $O_2(b, \upsilon = i) \rightarrow O_2(X, \upsilon' = i) + h\nu_i$. The intensity I_{bi-Xi} of the bi – Xi emission band is proportional

to the product $\sigma_i^3 q_{i,i} N_{bi}$ [115], where N_{bi} is the $O_2(b, v = i)$ concentration; σ_i and $q_{i,i}$ are the wave number and Franck – Condon coefficient for the $bi - Xi$ transition, respectively. The intensity of the P branch for the b2 – X2 transition is comparable with the noise of the measurement equipment. The P(b1 – X1) band is overlapped by the 774-nm emission band. The emission bands of transitions in the R branches are distinctly observed and are not overlapped by other emission bands. The relative concentrations of vibrationally excited molecules at the first (N_{b1}) and second (N_{b2}) vibrational levels were found from relations [80]

$$\eta_{b1} = \frac{N_{b1}}{N_{b0}} = \frac{\sigma_0^3 I_{R(b1-X1)} q_{00}}{\sigma_1^3 I_{R(b0-X0)} q_{11}}, \quad \eta_{b2} = \frac{N_{b2}}{N_{b0}} = \frac{\sigma_0^3 I_{R(b2-X2)} q_{00}}{\sigma_2^3 I_{R(b0-X0)} q_{22}},$$

where $I_{R(b-Xi)}$ is the R branch emission intensity for $v = i$. The fraction of vibrationally excited $O_2(b)$ molecules for the first and second vibrational levels at maximum was 22 % and 10 %, respectively [80].

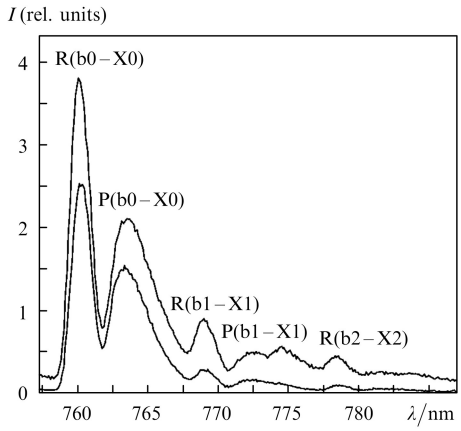


Figure 1. Emission spectra of $O_2(b)$ for $N_2 : O_2 : H_2O = 100 : 100 : 4$, $P_g \approx$ 35 Torr, $P_c = 3$ Torr, $L = 5$ cm, $\eta_\Delta = 60$ %, in the case of $\eta_{I_2} = 0.83$ % (the upper curve) and $\eta_{I_2} = 0.31$ % (the lower curve); R(bi – Xi) and P(bi – Xi) are the R and P emission bands of oxygen molecules corresponding to the $O_2(b, v = i) \rightarrow O_2(X, v' = i) + h\nu$ transitions [80].

The most complete list of processes involving $O_2(v)$ is presented in recent paper [124]. In this paper, the SKP [11] is supplemented with new processes and new kinetic data obtained in the last decade. The added processes are shown in Table 1 in bold [124]. The redistribution of vibrational quanta between oxygen molecules $O_2(a)$, $O_2(b)$, ad $O_2(X)$ occurs during rapid EE-exchange processes (89) – (93). As a result, the average number of vibrational quanta per each oxygen molecule [$O_2(X)$, $O_2(a)$ or $O_2(b)$] is virtually the same [78, 80]. The rate constants of the EE-exchange between $O_2(b, v = 1, 2, 3)$ with molecules $O_2(X)$ in processes (91) – (93) were measured in [125, 126]. One can see from Table 1 that they decrease with increasing v, which was explained in [125, 126] by the increase in the thermal effect of the reaction with increasing v. In [127], the rate constants of the EE-exchange between $O_2(a, v = 1, 2)$ and $O_2(X)$ molecules were measured [processes (89) and (90)].

The rate constants $K_{v'v''}^{O_2}$ of the VV-exchange in the process $O_2(X, v') + O_2(X, v'') \rightarrow O_2(X, v' - 1) + O_2(X, v'' + 1)$ were measured only for several values of v' and v''. In [128], the rate constant $K_{1,0}^{O_2} = 10^{-13}$ cm^{3}s^{-1} was calculated. The rates $K_{2,0}^{O_2} = 2 \times 10^{-13}$ cm^3 s^{-1} [process (76)] and $K_{3,0}^{O_2} = 2.6 \times 10^{-13}$ cm^3 s^{-1} [process (77)] were measured in [129]. Other rate constants $K_{v',v''}^{O_2}$ can be calculated from the relation $K_{v',v''}^{O_2} = 10^{-13}(v'' + 1)v''$ $\exp[-\delta_{VV}|v' + 1 - v''|] \times [1.5 - 0.5\exp(-\delta_{VV}|v' + 1 - v''|)]$ cm^3 s^{-1}, where $\delta_{VV} = 0.4(300/T)^{1/2}$ [130].

The specific feature of the kinetics of the active medium of the COIL is the low VT relaxation rate of $O_2(v)$ in collisions with O_2, N_2, H_2O molecules in processes (70) – (73). The vibrational energy of oxygen decreases mainly due to the VV′-exchange with H_2O molecules in process (85). This process plays an important role in the vibrational kinetics of oxygen. The models describing the dynamics of vibrationally excited oxygen in the atmosphere use the rate constant $K_{85} = 1.7 \times 10^{-12}$ cm^3 s^{-1} [131]. In [132], the value $K_{85} = 5.5 \times 10^{-13}$ cm^3 s^{-1} was recommended, which was obtained from the critical analysis of all the measurements of the rate constant of process (85). Vibrationally excited water molecules relax during rapid VT process (94).

Unfortunately, the distribution of energy released in processes (1), (3), (5), (9), (44), and (45) among reaction products is poorly known. A comparison of calculations with experimental data showed that about 4.5 vibrational quanta are formed during the quenching of one O_2 molecule in the active medium of the COIL [133, 134]. In [135], it is recommended to use the following probabilities $\gamma_{i,j}$ of vibrational excitation of reaction products (the excitation probability of the ith vibrational level of an O_2 molecule in the jth process from Table 1): $\gamma_{1,1} = 0$, $\gamma_{2,1} = 1$, $\gamma_{3,3} = 1$, $\gamma_{1,5} = 0$, $\gamma_{2,5} = 0$, $\gamma_{3,5} = 1$, $\gamma_{1,9} = 0$, $\gamma_{2,9} = 0$, $\gamma_{3,9} = 1$, $\gamma_{1,44} = 0$, $\gamma_{2,44} = 1$, $\gamma_{1,45} = 0$, $\gamma_{2,45} = 0$, and $\gamma_{3,45} = 1$. The values of $\gamma_{i,j}$ were chosen so that the total number of vibrational quanta produced during the quenching of one $O_2(a)$ molecule would not exceed 4.5.

Experiments and calculations showed [77 – 80, 122, 133 – 137] that the average number of vibrational quanta per one O_2 molecule can achieve $\eta_v = \sum_n n\eta_n \approx 0.3 - 0.4$ {$\eta_n = [O_2(v = n)]/[O_2]$ is the fraction of vibrationally excited O_2 molecules at the nth vibrational level, $n = 1, 2, 3 \ldots$}. In this connection, $O_2(a, v = 1)$ and $O_2(a, v = 2)$ molecules along with $O_2(a, v = 0)$ will be involved in the inversion of the laser transition in processes

$$O_2(a, v = 0) + I \leftrightarrow O_2(X, v = 0) + I^* + 279 \text{ cm}^{-1},$$

$$O_2(a, v = 1) + I \leftrightarrow O_2(X, v = 1) + I^* + 207 \text{ cm}^{-1},$$

$$O_2(a, v = 2) + I \leftrightarrow O_2(X, v = 2) + I^* + 131 \text{ cm}^{-1}.$$

The thermal effect of these reactions and, hence, the equilibrium constants of these processes decrease with increasing v. In this case, the threshold fractional content η_Δ^{th} increases with increasing the fraction of vibrationally excited O_2 molecules [134]. For example, the threshold yield of $O_2(a)$ for $\eta_v = 0.4$ at $T = 300$ K will be ~ 18 %, whereas for $\eta_v = 0$ it is 15 %. The gain in the medium decreases insignificantly with increasing η_v [134].

2.2 Production and relaxation of $I_2(v)$

Vibrationally excited iodine $I_2(X, v)$ produced in reaction (33) can play an important role in the dissociation of molecular iodine. The high relative concentrations of $I_2(X, v)$ in the oxygen–iodine medium were detected in several papers [118–120]. In [119], it was shown experimentally that vibrationally excited $I_2(X,\ 25 < v < 43)$ molecules were produced in reaction (33). The excited iodine atoms were generated by the photolysis of $I_2 - Ar$ mixtures at a wavelength of 475 nm or $CF_3I - I_2 - Ar$ at a wavelength of 266 nm. The $I_2(X, v)$ molecules were detected by the method of laser-induced fluorescence (LIF) at the $I_2(B \rightarrow X)$ transition. In [118, 120], $I_2(X, v)$ molecules were detected in the $I_2 - O_2(a) - O_2$ mixture also by the LIF method. In these experiments, $O_2(a)$ was produced in a discharge SOG, I_2 vapours being injected into the oxygen flow at the SOG output. Iodine molecules dissociated into atoms in collisions with $O_2(a)$ molecules, and excited atomic iodine was produced during EE energy transfer in process (40). In [118], the $I_2(X, v)$ molecules with vibrational quantum numbers in the range $33 \leqslant v \leqslant 44$ were detected. The authors of [120] have found experimentally the distribution of the absolute concentrations of iodine molecules over vibrational levels in the range $5 \leqslant v \leqslant 45$ (Fig. 2).

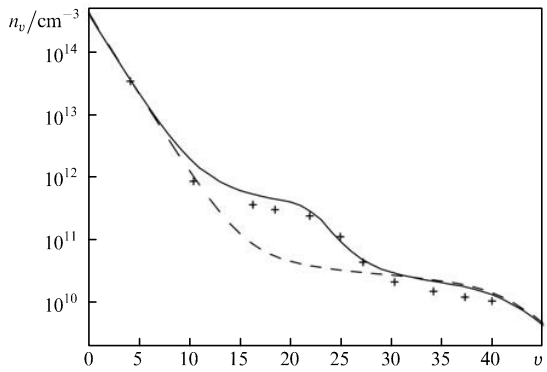


Figure 2. Populations of $I_2(X, v)$ molecules at a distance of 3 cm from the site of iodine injection into the oxygen flow under experimental conditions [120]: the initial composition of the mixture is $O_2(X):O_2(a):I_2 = 0.92:0.08:0.0475$ Torr, the initial flow rate is 10.8 m s^{-1}, and the initial temperature of the gas mixture is 300 K. The solid curve is calculated for $\Gamma_{v>24} = 0.1$ and $\Gamma_{15 \leqslant v \leqslant 24} = 0.9$, the dashed curve is calculated for $\Gamma_{v>24} = 0.1$ and $\Gamma_{15 \leqslant v \leqslant 24} = 0$; crosses are experimental data taken from [120].

To describe the vibrational excitation dynamics in molecular iodine, it is necessary to know the probabilities γ_v of producing $I_2(X)$ molecules at the vth vibrational level in reaction (33). The authors of paper [138] presented the distribution of γ_v over vibrational levels ($25 \leqslant v \leqslant 47$) in relative units, which was obtained from the measurements of the relative populations of $I_2(X, v)$. This distribution has a maximum at the level $v = 40$. By comparing the calculated concentrations $[I_2(X, v)]$ with experimental data obtained in [120], it was found that the total probability $\Gamma_{25 \leqslant v \leqslant 47} = \sum_{v=25}^{46} \gamma_v$ of producing $I_2(X, v > 24)$ molecules in reaction (33) was ~ 0.1, while the total probability of direct excitation of iodine molecules to vibrational levels with v from 15 to 24 was ~ 0.9 [139]. Figure 2 presents the calculated populations of $I_2(X, v)$ molecules for $\Gamma_{v>24} = 0.1$ and $\Gamma_{15 \leqslant v \leqslant 24} = \sum_{15}^{23} \gamma_v = 0.9$, and the measured concentrations $[I_2(X, v)]$. One can see that calculations well agree with experimental data. If we set $\Gamma_{15 \leqslant v \leqslant 24} = 0$ in calculations, then the calculated concentration of $I_2(X, 15 \leqslant v \leqslant 24)$ molecules (the dashed curve in Fig. 2) will be an order of magnitude lower than concentrations measured for $10 < v < 30$.

Analysis of the measured values of $[I_2(X, v)]$ showed that the distribution of γ_v over vibrational levels has two maxima: at $v = 40$ [138] and $v = 20 - 22$ [139]. The unusual two-maximum distribution of γ_v can be explained by two different mechanisms of reaction (33):

$$I_2(X) + I^* \rightarrow I_2(X, v > 24) + I,$$

$$I_2(X) + I^* \rightarrow I_3 \rightarrow I_2(X, 10 < v \leqslant 24) + I.$$

In the first channel of reaction (33), the $I_2(X, v > 24)$ molecules are produced during the EV energy transfer, which are distributed over vibrational levels as shown in Fig. 7 from paper [138]. The second channel of reaction (33) proceeds with the formation of the intermediate I_3 complex [64]. The obtained two-maximum distribution of γ_v suggests that branching ratios for the first and second channel of reactions (33) are equal to 0.1 and 0.9, respectively.

The relaxation rates of $I_2(X, v)$ molecules were studied in papers [138, 140]. The rate constants of the rotational–vibrational relaxation of $I_2(X, v, J)$ on components He, Ar, N_2, O_2, Cl_2, I_2, and H_2O are presented in [138] for the following combinations of vibrational (v) and rotational (J) levels: $v = 23$, $J = 57$; $v = 38$, $J = 49$, and $v = 42$, $J = 17$. At the first stage, the rotational–vibrational–electronic states of $I_2(B, v', J')$ were excited by pulsed radiation from a tunable dye laser pumped by a neodymium glass laser. A pulse from the second similar laser system excited the $I_2(B,\ v', J') \rightarrow I_2(X, v, J)$ transition, thereby populating the rotational–vibrational levels of the ground electronic state. The relative populations of the $I_2(X, v, J)$ states were measured by exciting the $X \rightarrow D$ transition by a probe laser pulse. For this purpose, the third tunable frequency-doubled dye laser was used. The relative populations of the $I_2(X, v, J)$ states were detected by LIF at the $I_2(X \rightarrow D)$ transition at ~ 321 nm. The relaxation rate constants of the $I_2(X, v, J)$ states were measured for $v = 23$, $J = 57$; $v = 38$, $J = 49$; and $v = 42$, $J = 17$ (see Table 1 in [138]). The VT-relaxation rate constants $K^M_{v,v-1}$ of iodine were determined for $v = 23$ and 38 and M = He, Ar, N_2, O_2, Cl_2, I_2, and H_2O from the numerical analysis of the LIF spectrum. The values of $K^M_{v,v-1}$ for $v = 23$ and 38 proved to be close. Because measurements were performed only for two values of v and their accuracy was low, the dependence of the VT-relaxation rate constant on the vibrational number was not found. The authors of [138] assumed that the value of in the relation $K^M_{v,v-1} = v^n K^M_{1,0}$ lies in the range 0–1. In [138], the values of $K^M_{v,v-1}$ were calculated for $n = 0$ and 1. The data for $n = 1$ are presented in Table 1 [processes (35)–(39)].

2.3 Kinetics of electronically excited $I_2(A', A, B)$ molecules

Intense yellow–green emission is observed when I_2 is added to a singlet-oxygen flow. The emission is caused by the $I_2(B) \rightarrow I_2(X)$ radiative transition. The excitation mechanism of $I_2(B)$ in the OIL active medium is not clear in detail. It was assumed in [26] that $I_2(B)$ was produced in

recombination process (63). The authors of [27, 28] showed that this recombination process cannot explain a number of features of the observed emission. They proposed another mechanism of the production of $I_2(B)$ in successive reactions (24) and (26).

The dependences of relative concentrations $[I_2(B)]$ downstream in a continuous-flow chamber for the $O_2(a)-I_2-N_2$ (or CO_2) mixture were recently obtained in [136] from the measurement of the emission intensity at the $I_2(B) \rightarrow I_2(X)$ transition. The emission intensity at maxima decreased inversely proportional to the N_2 (Fig. 3a) and CO_2 (Fig. 3b) pressures. This is caused by the collision-induced dissociation of $I_2(B)$ in process (27). According to the mechanism proposed in [28], the emission intensity at the $I_2(B \rightarrow X)$ transition should be inversely proportional to the square of the partial pressure of carbon dioxide because CO_2 efficiently quenches both $O_2(b)$ and $I_2(B)$. The observed emission intensity is virtually inversely proportional to the CO_2 pressure. This fact suggests that the role of $O_2(b)$ in the production of $I_2(B)$ is insignificant and the mechanism proposed in [28] is incorrect [136].

Note some features in the emission intensity distributions of molecular iodine in Fig. 3. The rise in the initial region is explained by the increase in the production rate of $I_2(B)$ in processes involving excited atomic iodine. When the maximum emission intensity is achieved at the $I_2(B \rightarrow X)$ transition, approximately 50 % of I_2 molecules have had time to dissociate [70]. The decrease in the emission intensity is caused by the decrease in the I_2 concentration due to dissociation.

It was expected that the luminescence of $I_2(B)$ should disappear after the termination of dissociation. In reality, however, a plateau in the emission intensity at the $I_2(B) \rightarrow I_2(X)$ transition was observed in the post-dissociation region (Fig. 3). Such a behaviour was also observed in [28, 70, 118]. The authors of [28] assumed that the stationary concentration of I_2 was maintained in the mixture due to recombination of atomic iodine on the chamber walls. This assumption was verified in [136] by inserting thin plates made of different materials into the gas flow behind the dissociation zone in order to increase the recombination rate of iodine atoms on the walls and, correspondingly, to increase the stationary concentration $[I_2]$. The emission intensity at the $I_2(B \rightarrow X)$ transition was virtually the same in the presence and absence of the plates. This suggests that the contribution of heterogeneous recombination to the production of $I_2(B)$ is insignificant.

By analysing the emission spectra of an oxygen–iodine medium, we can make some conclusions about the $I_2(B)$ production mechanism and its role in the dissociation of I_2. Figure 4 shows the typical emission spectrum of an oxygen–iodine medium in the visible region in the iodine dissociation zone. The emission spectrum in the wavelength range from 500 to 730 nm with a maximum at 570 nm belongs to molecular iodine emitting at the $I_2(B) \rightarrow I_2(X)$ transition. The emission spectrum behind the dissociation zone in the range from 500 to 730 nm is identical to the spectrum in Fig. 4, but its intensity is weaker by more than an order of magnitude [136]. The long-wavelength part of the spectrum in Fig. 4 between 750 and 800 nm exhibits the emission bands of oxygen at the $O_2(b, v') \rightarrow O_2(X, v'')$ transitions. Iodine molecules in the $I_2(B)$ excited electronic state can be produced upon recombination of I^* and I atoms in process (63) or during the EE energy transfer to $I_2(A, A')$ from singlet oxygen (26). The dominating quenching channel of $I_2(B)$ at gas pressures above 1 Torr is collision-induced dissociation (27). The concentration of $I_2(B)$ decreases insignificantly during spontaneous dissociation (30) and spontaneous emission (31) in the OIL active medium.

The concentration of $I_2(B)$ in an oxygen–iodine medium was estimated in [136] by comparing emission intensities at

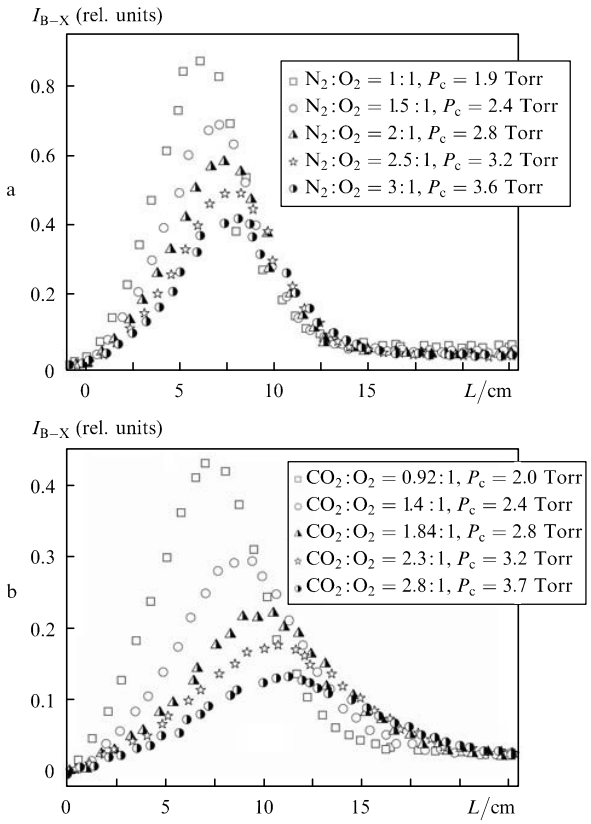


Figure 3. Distributions of the emission intensity of molecular iodine at the $I_2(B-X)$ transition along the coordinate L downstream for $\eta_\Delta = 60\,\%$, $\eta_w = 3\,\%$, and $\eta_{I_2} = 0.28\,\%$ for the oxygen–iodine mixture diluted with nitrogen (a) and carbon dioxide (b) [136].

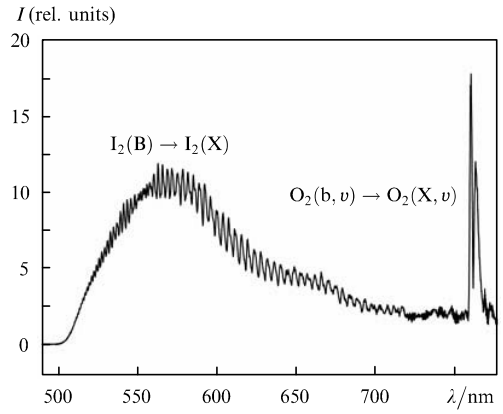


Figure 4. Emission spectrum of the oxygen–iodine medium in the I_2 dissociation zone for $P_g \approx 35$ Torr, $P_c = 2.3$ Torr, $\eta_{I_2} = 0.5\,\%$, $\eta_\Delta = 60\,\%$, $\eta_w = 3\,\%$, $L = 4$ cm and $N_2:O_2 = 1:1$ [136].

the $I_2(B-X)$ and $O_2(b-X)$ transitions. The ratios I_{B-X}/I_{b-X} of the integrated emission intensities at the $I_2(B-X)$ and $O_2(b-X)$ transitions are equal to ~ 21.8 in the dissociation zone and ~ 2.3 behind this zone. On the other hand, the ratio of the emission intensities at the $I_2(B-X)$ and $O_2(b-X)$ transitions is related to concentrations $[I_2(B)]$ and $[O_2(b)]$ by the expression

$$\frac{I_{B-X}}{I_{b-X}} = \frac{[I_2(B)]\Gamma_B}{[(O_2(b)]\Gamma_b},$$

where $\Gamma_B = 6 \times 10^5$ s^{-1} and $\Gamma_b = 0.08$ s^{-1} are the radiative decay rates of $[I_2(B)]$ and $[O_2(b)]$, respectively. The approximate concentration of $O_2(b)$ molecules under experimental conditions corresponding to Fig. 4 is 10^{14} cm^{-3} [135]. This gives the estimate of the concentration $[I_2(B)]$ in the dissociation zone equal to 3.5×10^8 cm^{-3}. This value should be three orders of magnitude higher to provide the experimental dissociation rate [135] of iodine caused only by reaction (27). Thus, the role of $I_2(B)$ in the dissociation process is insignificant [136]. It is most likely that the dissociation of iodine involves the unbound $I_2(^1\Pi_{1u})$ state produced in the process $I_2(A, A') + O_2(a) \rightarrow I_2(^1\Pi_{1u}) + O_2(X)$. In addition, $I_2(A, A')$ molecules dissociate in 'thermal' collisions in reactions (29.2) and (29.4) [141].

By assuming that $I_2(B)$ is produced due to recombination (63), the intensity ratio I_{B-X}/I_{b-X} can be estimated as ~ 3.5 [136]. Thus, the recombination rate does not provide the required production rates of $I_2(B)$ in the dissociation zone, but can provide them behind this zone [136].

Recently the mechanism of production of $I_2(B)$ was proposed [136] which involves the $I_2(A', A)$ excited electronic states populated in collisions of $I_2(X)$ with $O_2(a, v = 1, 2)$ molecules [processes (95) and (96)] or $I_2(X, 11 \leqslant v \leqslant 24)$ with $O_2(a)$ [process (101)]. Figure 5 illustrates the production mechanism of the A′ and A states of I_2 molecules [arrows (95), (96), and (101)], the mechanism of production of vibrationally excited $I_2(X)$ molecules at vibrational levels in the range $11 \leqslant v \leqslant 24$ [arrow 0.9(33)], and pumping of $I_2(B)$ from the A′ and A states [arrow (26)].

The emission spectrum at the $I_2(B) \rightarrow I_2(X)$ transition (Fig. 4) has the same structure in the dissociation zone and behind it. This means that the production mechanisms of $I_2(B)$ in both zones are similar. The production mechanism of $I_2(B)$ in the dissociation zone includes processes (95), (96), (101), and (26) involving the intermediate $I_2(A, A')$ state. In the post-dissociation zone, the production mechanism of $I_2(B)$ is the same. During homogeneous recombination (62), a very low stationary concentration of $I_2(X)$ molecules is maintained. This explains the presence of a plateau in the dependence of the emission of iodine on the coordinate along the flow in the post-dissociation zone (see Fig. 3).

The deactivation kinetics of $I_2(A')$ in collisions with CO_2, Ar, O_2, H_2O, and I_2 was studied in papers [135, 141, 142]. The A′ state was excited by using the following scheme. At the first stage, the $I_2(X) \rightarrow I_2(D)$ transition was excited by 10-ns, 193-nm pulses from an excimer laser. Then, $I_2(D')$ molecules were produced in collisions of $I_2(D)$ with argon, which passed to the A′ state due to the spontaneous $I_2(D') \rightarrow I_2(A') + h\nu$ transition [141]. A probe pulse from a tunable dye laser excited the $D \leftarrow A'$ transition. Laser pulses at ~ 285 nm were obtained by frequency doubling. The time delay between laser pulses

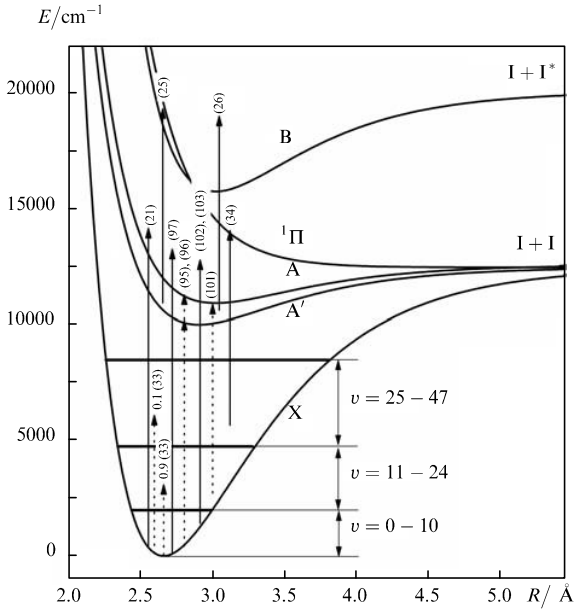


Figure 5. Potential energy curves of the I_2 molecule. The dotted and solid straight lines show the excitation channels of states lying below and above the I_2 dissociation limit, respectively. The numbers of processes from Table 1 are shown above the arrows.

was controlled with a delay generator. A LIF signal at the $I_2(D') \rightarrow I_2(A')$ transition at 340 nm was separated with a monochromator and detected with a photomultiplier. The measured quenching rates for $I_2(A')$ are presented in Table 1 [processes (28)–(29.4)]. It is interesting that the rate constant of quenching of $I_2(A')$ by a homonuclear oxygen molecule (6.3×10^{-12} cm^{3}s^{-1}) exceeds the rate constants of quenching by CO_2 and H_2O molecules. Based on this fact, it is argued in [135] that the high rate of quenching of $I_2(A')$ by O_2 molecules is caused by the EE energy transfer in the process $I_2(A') + O_2(X) \rightarrow I_2(X) + O_2(a)$, which can also lead to the formation of vibrationally excited products. This process, which is important for the understanding of the dissociation mechanism of I_2 in the OIL active medium, was also observed in experiments with the use of argon matrices with additions of I_2 and O_2 (at cryogenic temperatures) [143].

2.4 Dissociation channels of I_2 in the active medium of an oxygen–iodine laser

The dissociation mechanism of I_2 in OILs is not explained so far. The excitation energy of $O_2(a)$ (7882 cm^{-1}) is insufficient for the dissociation of the I_2 molecule (12441 cm^{-1}) during one collision. It has been established reliably that the dissociation process has the chain and initiating stages and involves an intermediate excited state of I_2. However, it is not clear which of the excited states of I_2 is intermediate, and the pumping mechanism of this state is unknown. Several dissociation mechanisms of I_2 in the OIL medium have been proposed.

The authors of [27, 28] assume that I_2 dissociates in collisions with $O_2(b)$ (13121 cm^{-1}) in process (21). This process with the gas-kinetic rate constant well explains the dissociation dynamics in experiments with a continuous-flow chamber [70]. Direct measurements [74] showed that the rate constant K_{21} is much smaller than the gas-kinetic

rate constant, and, therefore, the rate of process (21) cannot provide the dissociation rate of I_2 observed experimentally. The recent measurement [75] of the rate constant K_{21} gave the value 3.5×10^{-11} cm^3 s^{-1} which exceeds its value 4×10^{-12} cm^3 s^{-1} obtained earlier [74]. However, both these values are much lower than that required by the dissociation model proposed in [27, 28]. The rate of process (21) is much lower than the dissociation rates of iodine observed both at the chain and initiating stages [135, 144].

The SKP [11] uses the mechanism proposed in [70] in which dissociation at the initiating stage proceeds through processes (32) and (34). The intermediate state in this model is the $I_2(X, v)$ molecule in the ground electronic state with vibrational quantum numbers above $v = 23$. The initiating stage is followed by the chain reaction described by the sequence of reactions (40), (33), and (34). However, the recent experimental data cast doubt on this dissociation mechanism. The values of the rate constants of reactions deactivating the intermediate state in SKP [11] are more suitable for the quenching of excited electronic state [55, 68] rather than $I_2(X, v)$. In addition, the directly measured rate constant of quenching of $O_2(a)$ by molecules $I_2(X)$ [process (32)] is at least an order of magnitude lower [69] than assumed in SKP [11]. It was recently shown [139] that the total probability $\Gamma_{v>23}$ of the production of molecules $I_2(X, v > 23)$ during the quenching of I^* by $I_2(X)$ molecules is ~ 0.1. The standard dissociation model with this value of the probability does not provide the decomposition rates of I_2 observed in experiments. In addition, according to this model, the number of singlet oxygen molecules required for the dissociation of one I_2 molecule should exceed 20, which contradicts experimental data.

Arnold et al. [26] assumed that electronically excited $I_2(A', A)$ can be involved in dissociation in the sequence of reactions

$$O_2(a) + I_2(X) \rightarrow O_2(X) + I_2(A', A),$$

$$O_2(a) + I_2(A', A) \rightarrow O_2(X) + 2I.$$

The lower excited electronic states of iodine are the $A'\,^3\Pi_{2u}$ and $A\,^3\Pi_{1u}$ states with energies 10047 and 10847 cm^{-1}, respectively. The energy difference of the states $O_2(a)$ and $I_2(A', A)$ greatly exceeds the thermal collision energy. Therefore, the EE energy transfer from $O_2(a)$ cannot provide the required population rate of $I_2(A', A)$. Note, however, that electronically excited $I_2(A', A)$ molecules were detected in the $O_2(a)$–I_2 mixture [70, 143, 145, 146]. David [145] observed emission at the $I_2(A \rightarrow X)$ transition when molecular iodine vapours were added to a $O_2(a)$ molecular flow. Heidner et al. [70] also observed luminescence at the $I_2(A \rightarrow X)$ transition in the $O_2(a)$–I_2 gas mixture. The lower excited $I_2(A')$ electronic state is metastable and cannot be observed with the help of emission spectroscopy. The $I_2(A')$ state was observed in the $O_2(a)$–I_2 mixture using LIF detection of the $D' - A'$ transition.

The excitation mechanism of the A' and A states in the $O_2(a)$–I_2 mixture is not established. We can assume that the energy difference between the $I_2(A', A)$ and $O_2(a)$ states is compensated by the vibrational excitation energy of singlet oxygen. This assumption is confirmed by papers [77–80, 122, 133–136] in which high nonequilibrium concentrations of $O_2(X, v)$, $O_2(a, v)$, and $O_2(b, v)$ in the OIL active medium were detected. Vibrationally excited O_2 can be involved in the dissociation of I_2 in energy-exchange processes (95) and (96). The thermal effect of processes (95) and (96) (623 and 23 cm^{-1}, respectively) can be compensated by the kinetic energy of colliding particles. In this case, the rates of these reactions can provide the required dissociation rate of I_2. The energy stored in $O_2(a, v = 3)$ is sufficient to cause the dissociation of I_2 in one collision [76].

The dissociation model in which intermediate states are the lower excited electronic states A' and A of the I_2 molecule pumped during energy-exchange processes (95) and (96) was called the LAH (Lilenfeld–Azyazov–Heaven) model [144]. This model well describes the dissociation rate of iodine in experiments with a continuous-flow chamber [135] in which the initial concentration of I_2 in the iodine flow was only twice as large as that in the completely mixed flow. The local concentration of I_2 vapours in jets injected into the oxygen flow in real mixing devices is much higher than that in the completely mixed flow. Under these experimental conditions [144], the dissociation rates are much higher than that predicted by the LAH model. The authors of [144] supplemented the LAH model with processes from the Heidner model [70]:

$$I_2(X) + I^* \rightarrow I_2(X, v > 23) + I,$$

$$I_2(X, v \geqslant 23) + O_2(a) \rightarrow I + I + O_2(X),$$

$$I_2(X, v \geqslant 23) + M \rightarrow I_2(X) + M.$$

The model combined in this way was called the HLAH model [144]. The dissociation rate of iodine at the initiating stage was provided by processes included into the LAH model, while at the chain stage – by process included into the Heidner model. The three-dimensional calculations of the flow of a reacting gas mixture based on the Navier-Stokes equations and HLAH model well describe the dissociation rate of iodine in a supersonic COIL [144]. It was assumed in these calculations that the total probability of producing $I_2(X, v > 23)$ in process (33) is unity. However, it was shown recently [139] that this probability is an order of magnitude smaller. Thus, the HLAH model also cannot provide the dissociation rate of iodine observed experimentally.

The LAH model was further developed in paper [124], where it was assumed that the intermediate $I_2(A', A)$ states are excited, additionally to processes (95) and (96), in collisions of vibrationally excited molecules $I_2(X, 11 \leqslant v \leqslant 24)$ with $O_2(a)$ [process (101)]. Molecules $I_2(X, 11 \leqslant v \leqslant 24)$ are produced in process (33) with the quantum yield 0.9 [139]. The developed model also includes the direct dissociation of iodine in collisions with $O_2(b)$ with the rate constant $K_{21} = 3.5 \times 10^{-11}$ cm^{3}s^{-1} [75]. Note in addition that the total energy of colliding particles in processes (97), (102) and (103) exceeds the dissociation energy of I_2. The contribution of these channels to dissociation increases with increasing the fraction of vibrationally excited O_2 and I_2 molecules in the mixture. It is most likely that the dissociation of iodine in the presence of $O_2(a)$ proceeds simultaneously over several channels, as follows from Fig. 5. The dashed arrows show the excitation channels of intermediate states, while the solid arrows show the dissociation channels of iodine.

The multiparametric experimental investigation of the dissociation kinetics of iodine in singlet oxygen was performed in [135] by the emission method in a low-pressure continuous-flow chamber. The concentration profiles of excited states along the flow were measured in a broad range of mixture compositions. Figure 6 demonstrates the distributions of the concentration of excited I^* atoms along the coordinate L of the flow for oxygen diluted with nitrogen at the ratio $O_2:N_2 = 1:1$, the relative content of water vapours in oxygen $\eta_w = [H_2O]/[O_2] \approx 3\,\%$ and the relative fraction of $O_2(a)$ $\eta_\Delta = 60\,\% \pm 10\,\%$ for several relative concentrations of I_2 in the range $\eta_{I_2} = 0.18\,\%$–$1.44\,\%$. The figure also presents the I^* concentration distributions (solid curves) calculated by using multichannel dissociation [124] under conditions employed in experiments. The calculated data proved to be rather sensitive to the values of K_{101} and η_Δ. The satisfactory agreement between calculations and experiment was achieved for $K_{101} = 10^{-12}$ cm^3 s^{-1} and $\eta_\Delta = 60\,\%$.

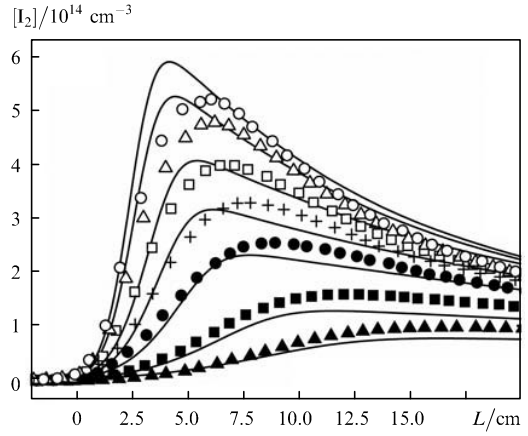


Figure 6. Dependences of the concentration of I^* on the coordinate L along the flow for $\eta_w = 3\,\%$, $\eta_\Delta = 60\,\% \pm 10\,\%$, $N_2:O_2 = 1:1$ for the following conditions: $\eta_{I_2} = 1.44\,\%$, $P_c = 2.2$ Torr (○); $\eta_{I_2} = 1.23\,\%$, $P_c = 2.2$ Torr (△); $\eta_{I_2} = 0.94\,\%$, $P_c = 2.1$ Top (□); $\eta_{I_2} = 0.7\,\%$, $P_c = 2.1$ Torr (+); $\eta_{I_2} = 0.52\,\%$, $P_c = 2.0$ Torr (●); $\eta_{I_2} = 0.29\,\%$, $P_c = 1.9$ Torr (■); $\eta_{I_2} = 0.18\,\%$, $P_c = 1.8$ Torr (▲). The curves are calculated for $\eta_\Delta = 60\,\%$ and $K_{101} = 10^{-12}$ cm^3 s^{-1} [135].

The local concentration of I_2 in jets injected into the oxygen flow in real laser systems is much higher than the iodine concentration in the completely mixed flow. The authors of [147] found that the multichannel dissociation model with the rate constant $K_{101} = 10^{-12}$ cm^3 s^{-1} predicted the dissociation rate that was six times lower than that observed in their experiments [144]. They concluded that the rate constant of process (101) should be an order of magnitude higher. However, the model with $K_{101} = 10^{-11}$ cm^3 s^{-1} predicts considerably overstated dissociation rates for experiments with a continuous-floe chamber [135]. This discrepancy in the values of K_{101} can be explained by the measurement error of η_Δ, which was $\pm 10\,\%$. The multichannel dissociation model [124] also provides satisfactory agreement with experiments [135] for $\eta_\Delta = 50\,\%$ and $K_{101} \approx 10^{-11}$ cm^3 s^{-1}. It is most likely that K_{101} lies in the range from 10^{-12} to 10^{-11} cm^3 s^{-1}.

The analysis of the calculation results showed that the greater part of iodine molecules passes during dissociation through the A′ and A states, which are excited in processes (95) and (96) involving vibrationally excited oxygen and in process (101) involving vibrationally excited $I_2(X, 11 \leqslant v \leqslant 24)$ [124]. Processes (95), (96), and (25) provide dissociation at the initiating stage. The contribution of this sequence of processes to dissociation at the chain stage is predominant for the relative initial local concentrations of iodine $\eta_{I_2} < 1\,\%$, while the contribution of process (101) is significant only at the chain stage and only for $\eta_{I_2} \geqslant 1\,\%$. Thus, the dissociation of I_2 is an example of the process involving both vibrationally and electronically excited states. The dissociation channel proposed in [70] gives a small contribution for the total probability of producing $I_2(X, v \geqslant 25)$ in process (33) equal to $\Gamma_{v \geqslant 25} = 0.1$. The contribution of the direct dissociation of iodine in processes (21), (97), (102), and (103) is also insignificant.

3. Excitation and deactivation kinetics of $O_2(a)$ and I^* in the active media of electric-discharge and photolysis oxygen–iodine lasers

Processes of the excitation and deactivation of $O_2(a)$ in electric-discharge plasmas have been extensively studied in papers [21, 22, 31–41, 148–151]. The yield of excited $O_2(a)$ molecules at the exit of the discharge zone is mainly determined by the excitation and deactivation of oxygen in collisions with plasma electrons. The total kinetic scheme of processes in the electric-discharge OIL medium is presented in papers [22, 32, 150]. The analysis of plasma-chemical processes in mixtures containing oxygen showed that the optimal value of η_Δ is obtained for $E/N \approx 10$ Td [21, 22, 31, 32, 150] (E is the electric field strength and N is the gas number density).

Discharges of numerous types used in OILs include the dc discharge [149], radio-frequency [32–34, 36–38, 41, 148] and microwave [35] discharges, and nonself-sustained discharges induced by an electron beam [31] and pulsed preionisation [40, 151]. The nonself-sustained discharge can be realised in regimes with the low reduced field ($E/N \leqslant 10$ Td) at oxygen pressures of a few tens of torr [31, 40]. The nonself-sustained discharge maintained by an external electron beam remains stable at energy inputs of 150 kJ mol^{-1} in the $O_2 - Ar - CO$ mixture with the total pressure of 30 Torr [31]. It was shown theoretically in [31] that the maximum yield of $O_2(a)$ in the discharge of this type can achieve 25%. Recently, the authors of [40] studied the characteristics of the nonself-sustained discharge induced by pulsed preionisation in the $O_2:He = 1:10$ mixture at the total pressure of 120 Torr. However, the yield η_Δ was low, being only 6%. The relatively large value of η_Δ ($\sim 30\,\%$) was obtained in [151] by using external preionisation at the total pressure of the gas mixture 60–100 Torr.

The fraction of singlet oxygen at the output of electric-discharge SOGs is in the best case equal to or slightly exceeds the threshold yield η_Δ^{th} at room temperature. The threshold yield of $O_2(a)$ decreases as the gas temperature is decreased. The positive gain can be obtained even for $\eta_\Delta \approx 15\,\% - 20\,\%$ by using the cooling of gas upon adiabatic expansion in a supersonic nozzle. A comparatively low pressure of oxygen at the output of an electric-discharge SOG (several torr) could not provide a high gain [33, 35]. To increase the efficiency of an EOIL, it is necessary to increase the oxygen pressure at the generator output up to a few tens of torr. However, the increase in the O_2 pressure is

accompanied by a decease in the gain, which is caused by the presence of $O(^3P)$ atoms at the output of the electric-discharge SOG.

Atomic oxygen plays a double role in an EOIL. It accelerates the dissociation of molecular iodine, but also deactivates both $O_2(a)$ and I^*. As shown in [22, 23], the yield of $O_2(a)$ decreases with increasing oxygen pressure. The authors of these papers assume that the increase in the deactivation rate of $O_2(a)$ with increasing the O_2 pressure is caused by three-body process (2.38). (Processes considered in section 3 are presented in Table 2.) To provide the removal rate of $[O_2(a)]$ observed in these experiments, the rate constant $K_{2.38}$ of process (2.38) should be in the range $(1-3)\times10^{-32}$ cm^6 s^{-1}.

Table 2. Additional processes typical for EOILs and POILs and their rate constants.

Reaction number	Reaction	Rate constant *	References
2.1	$O_3 + h\nu \rightarrow O(^1D) + O_2(a)$	0.9 **	[155]
	$O_3 + h\nu \rightarrow O(^3P) + O_2(X)$	0.1 **	[155]
2.2	$CF_3I + h\nu \rightarrow CF_3 + I^*$	0.89 **	[156]
	$CF_3I + h\nu \rightarrow CF_3 + I$	0.11 **	[156]
2.3	$N_2O + h\nu \rightarrow O(^1D) + N_2$	0.995**	[157]
2.4	$O(^1D) + N_2O \rightarrow NO + NO$	7.6×10^{-11}	[157]
2.5	$O(^1D) + N_2O \rightarrow N_2 + O_2(a)$	4.3×10^{-11}	[157]
2.6	$O(^1D) + N_2O \rightarrow O(^3P) + N_2O$	6.0×10^{-12}	[157]
2.7	$O_2(a) + I \rightarrow O_2(X) + I^*$	7.8×10^{-11}	[11]
2.8	$O_2(X) + I^* \rightarrow O_2(a) + I$	2.7×10^{-11}	[11]
2.9	$I^* + O_2(a) \rightarrow I + O_2(b)$	1.1×10^{-13}	[11]
2.10	$I^* + O_2(a) \rightarrow I + O_2(a)$	1.1×10^{-13}	[11]
2.11	$I^* + I_2(X) \rightarrow I + I_2(X)$	3.8×10^{-11}	[11]
2.12	$I^* + O(^3P) \rightarrow I + O(^3P)$	1.2×10^{-11}	[158]
2.13	$I^* + NO_2 \rightarrow I + NO_2$	2.9×10^{-15}	[159]
2.14	$I^* + N_2O_4 \rightarrow$ products	3.5×10^{-13}	[159]
2.15	$I^* + N_2O \rightarrow I + N_2O$	1.4×10^{-15}	[159]
2.16	$I^* + IO \rightarrow I + IO$	?	
2.17	$I^* + O_3 \rightarrow$ products	1.8×10^{-12}	[158]
2.18	$I + O_3 \rightarrow IO + O_2$	1.2×10^{-12}	[157]
2.19	$I_2(X) + O(^3P) \rightarrow IO + I$	1.4×10^{-10}	[160]
2.20	$IO + O(^3P) \rightarrow O_2(X) + I$	1.5×10^{-10}	[160]
2.21	$IO + IO \rightarrow I + IO_2$	3.2×10^{-11}	[157]
2.22	$IO + IO \rightarrow 2I + O_2$	8.0×10^{-12}	[157]
2.23	$IO + NO \rightarrow I + NO_2$	1.82×10^{-11}	[157]
2.24	$O(^1D) + N_2 \rightarrow O(^3P) + N_2$	2.6×10^{-11}	[157]
2.25	$O(^1D) + CO_2 \rightarrow O(^3P) + CO_2$	1.3×10^{-10}	[161]
2.26	$O(^1D) + Ar \rightarrow O(^3P) + Ar$	5.0×10^{-13}	[161]
2.27	$O(^1D) + O_2 \rightarrow O(^3P) + O_2(X, a, b)$	4.0×10^{-11}	[157]
2.28	$O(^3P) + NO_2 \rightarrow O_2(X, a) + NO$	1.0×10^{-11}	[157]
2.29	$O_2(a) + IO \rightarrow O_2(X) + IO$	?	
2.30	$O_2(a) + O_3 \rightarrow O_2(X) + O_3$	3.8×10^{-15}	[150]
2.31	$O_2(a) + O(^1D) \rightarrow O_2(X) + O(^3P)$	1.0×10^{-11}	[150]
2.32	$O_2(a) + O(^3P) \rightarrow O_2(X) + O(^3P)$	7.0×10^{-16}	[22]
2.33	$O_2(a) + CF_3O \rightarrow O_2(X) + CF_3O$	4.5×10^{-11}	[162]
2.34	$O_2(b) + O_3 \rightarrow$ products	1.9×10^{-11}	[163]
2.35	$O_2(b) + O(^3P) \rightarrow O_2(X, a) + O(^3P)$	8.0×10^{-15}	[150]
2.36	$O(^3P) + O_2 + Ar \rightarrow O_3 + Ar$	4.0×10^{-34} cm^6 s^{-1}	[164]
2.37	$O(^3P) + O_2 + O_2 \rightarrow O_3 + O_2$	6.0×10^{-34} cm^6 s^{-1}	[157]
2.38	$O(^3P) + O_2(a) + O_2 \rightarrow O(^3P) + 2O_2$	1.1×10^{-31} cm^6 s^{-1}	[163]
2.39	$O(^3P) + NO + M \rightarrow NO_2^* + M$	1.0×10^{-31} cm^6 s^{-1}	[157]

Notes: *If the dimensionality is not presented, the rate constant is measured in cm^3 s^{-1}; **the quantum yield of process in UV photolysis.

The quenching of I^* by $O(^3P)$ atoms in the post-discharge zone was investigated in [33, 35], where the distributions of the concentration of I^* and the gain of the medium along the flow were recorded. It was found that the electronic-energy relaxation rate drastically decreased after the addition of NO_2 molecules to the flow. NO_2 molecules react with atomic oxygen in process (2.28) and bound it. It was assumed that electronic energy is relaxed in process (2.12). The authors of papers [33, 35] simulated the kinetics of processes in the post-discharge zone and estimated the rate constant $K_{2.12}$ of process (2.12) as $(0.4-1.0)\times10^{-11}$ cm^3 s^{-1}. Positive gains were obtained by adding molecular iodine vapours into the gas flow emerging from the electric-discharge SOG both in the supersonic [33] and subsonic [35] flow regimes. In these papers, radio-frequency [33] and microwave [35] discharges were used. Lasing was first obtained with an electric-discharge SOG in which a radio-frequency discharge was used [34]. The output power of the EOIL was 220 mW. The output power was later increased up to 12.3 W [152].

The possibility of using the UV photolysis of O_3 for producing $O_2(a)$ in POILs was considered in papers [153, 154]. The quantum yield of $O_2(a)$ obtained in the UV photolysis of O_3 in process (2.1) is close to 90 % [155], which makes this method for exciting the $I^* \rightarrow I$ laser transition promising. The emission of an OIL upon pulsed photolysis of ozone by the 264-nm fourth harmonic of a neodymium glass laser was first obtained in paper [154]. The energy extraction from the $CF_3I:O_3:SF_6:He:N_2O = 0.055:0.45:11:21:6$ Torr mixture was 0.8 mJ cm^{-3} for the conversion efficiency of the $O_2(a)$ energy to laser radiation of about 41 %. A specific feature of the photolysis SOG is the high concentration of photolysis products $O(^1D)$ and $O(^3P)$ and of residual O_3. The $O(^1D)$ atoms efficiently quench both $O_2(a)$ and I^* [154]. These atoms were removed from the mixture by using NO_2, CO_2 and N_2 [processes (2.4)–(2.6), (2.24) and (2.25)]. The N_2O molecules react with $O(^1D)$ in chemical reactions (2.4)–(2.6), by removing atomic oxygen from the mixture. The laser pulse energy in mixtures containing N_2O was considerably higher than in mixtures with CO_2 and N_2. It was assumed [154] that atomic oxygen efficiently quenches I^* in process (2.12) and $O_2(a)$ is produced in process (2.5), although these assumptions were not confirmed directly. In addition, undissociated ozon also quenches I^* in process (2.17).

Although a photolysis OIL provides the high quantum yield of $O_2(a)$, it has not gained wide acceptance because of the instability of the initial reagent (ozone) and the low conversion efficiency of light energy to the excitation energy of $O_2(a)$, which is caused by a great difference between the UV photon energy and the $O_2(a)$ excitation energy.

3.1 Quenching of $O_2(a)$ in the $O(^3P)-O_2(X)-O_2(a)$ mixture

The deactivation rate of singlet oxygen in mixtures containing oxygen atoms and molecules was measured directly in [163] by the method of pulsed laser photolysis (PLP) of the $O_3-O_2-Ar-CO_2$ mixture at a wavelength of 248 nm. Oxygen atoms and singlet oxygen molecules were produced by ozone photolysis in process (2.1). The deactivation rate of $O_2(a)$ was determined from the time profiles of radiation intensity at the $O_2(a-X)$ transition.

Figure 7 shows the typical time dependence of the radiation intensity of $O_2(a)$ at 1268 nm after the PLP of the $O_2 - O_3 - Ar$ mixture at the oxygen pressure $P_{O_2} =$ 680 Torr, the partial pressure of argon $P_{Ar} = 90$ Torr, the initial pressure of ozone $P_{O_3} = 2.4$ Torr, $T = 300$ K, and the laser pulse energy density $E_{las} = 80$ mJ cm^{-2}.

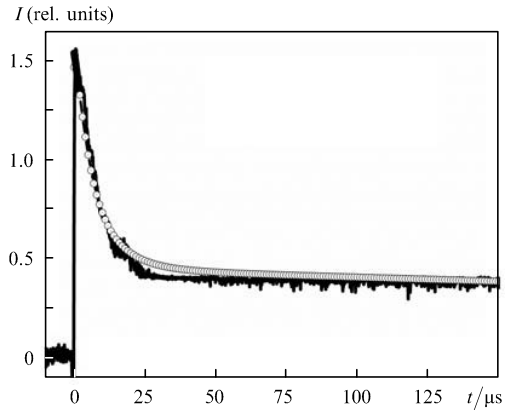


Figure 7. Typical time dependence of the emission intensity of $O_2(a)$ molecule after the laser photolysis of the $O2 - O_3 - Ar$ mixture for $P_{O_2} = 680$ Torr, $P_{Ar} = 90$ Torr, $P_{O_3} = 2.4$ Torr, $E_{las} = 80$ mJ cm^{-3} and $T = 300$ K (solid curve). Points are calculated for experimental conditions and $K_{2.38} = 1.1 \times 10^{-31}$ cm^6 s^{-1} [163].

The time profiles of the concentration of atomic oxygen were found from the chemiluminescence reaction $O + NO + M \rightarrow NO_2^* + M + h\nu$. For this purpose, a small amount of nitrogen oxide N_2O was added to the $O_2 - O_3 - Ar$ mixture. The NO molecules were produced in rapid chemical reaction (2.4). Figure 8 shows the time dependence of the emission intensity of the chemiluminescence reaction at 600 nm after the PLP of the $O_2 - O_3 - Ar - N_2O$ mixture at 248 nm for $P_{O_2} = 654$ Torr, $P_{Ar} = 108$ Torr, $P_{O_3} = 2.5$ Torr, $P_{N_2O} =$ 2.8 Torr, $E_{las} = 80$ mJ cm^{-2}, and $T = 300$ K. It follows from calculations that the concentration of NO molecules

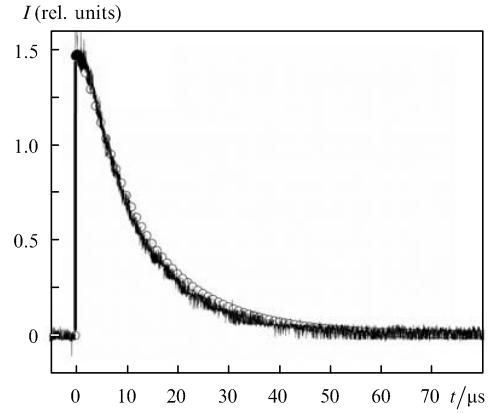


Figure 8. Time profile of the emission intensity at 600 nm in the chemiluminescence reaction after the PLP of the $O_2 - O_3 - Ar - N_2O$ mixture at 248 nm for $P_{O_2} = 654$ Torr, $P_{Ar} = 108$ Torr, $P_{O_3} = 2.5$ Torr, $P_{N_2O} =$2.8 Torr, $E_{las} = 80$ mJ cm^{-2} and $T = 300$ K. Points are the calculated values of the product [O][NO] [163].

was almost constant during the observation time, and, therefore, the time dependence of the emission intensity corresponds to the time dependence of the relative concentration of $O(^3P)$ atoms.

We can distinguish two parts in the time dependence of the oxygen emission at the $O_2(a) \rightarrow O_2(X)$ transition in Fig. 7. In the initial part of the curve, in the time interval up to 20 μs, the emission intensity drastically decreases approximately by four times. For $t > 20$ μs, the emission intensity profile is smoother, which is well explained by the relaxation of $O_2(a)$ in collisions with ozone in process (2.30). The rapid relaxation of $O_2(a)$ at the time scale of no more than 20 μs is unusual because singlet oxygen molecules are very weakly deactivated in collisions.

One can see from Fig. 8 that $O(^3P)$ atoms recombine in process (2.37) during the time approximately equal to the decay time of the $O_2(a)$ concentration at the initial part of the curve in Fig. 7. The rapid quenching of $O_2(a)$ takes place only in the presence of $O(^3P)$ atoms. This confirms the assumption [22, 32] that the rapid quenching of $O_2(a)$ in the presence of oxygen atoms is caused by three-body process (2.38). Experimental data on the deactivation of $O_2(a)$ were processed taking this assumption into account. The decay rate of $[O_2(a)]$ at the initial part of the curve was well described by calculations with the rate constant $K_{2.38} = 1.1 \times 10^{-31}$ cm^6 s^{-1} [163]. This value is considerably higher than values $K_{2.38} = (1 - 3) \times 10^{-32}$ cm^6 s^{-1} obtained in [22, 32] by simulations of kinetic processes in the post-discharge zone.

The time profiles of the $O_2(a)$ emission intensity at 1268 nm were obtained for different compositions of the $O_2 - O_3 - Ar - CO_2$ mixture. The deactivation rate of $O_2(a)$ remained invariable at different partial pressures of Ar. This contradicts the data obtained in papers [22, 32]. The authors of these papers found that the relaxation rate of $O_2(a)$ in the post-discharge zone increased with increasing the content of Ar in the initial mixture. They explained this fact by the quenching of $O_2(a)$ in the process $O(^3P) + O_2(a) + Ar \rightarrow O(^3P) + O_2 + Ar$ with the rate constant of $0.63K_{2.38}$.

Vibrationally excited ozone $O_3(v = 1)$ deactivates $O_2(a)$ in the reaction $O_3(v = 1) + O_2(a) \rightarrow 2O_2 + O$ 38 times more rapidly than unexcited ozone ($v = 0$) [165]. In processes (2.36) and (2.37), about five vibrational quanta are produced at different modes of O_3. We can assume that vibrationally excited ozone with $v > 1$ can quench $O_2(a)$ more efficiently. This mechanism should be taken into account in the interpretation of the rapid relaxation of $O_2(a)$ in the presence of atomic and molecular oxygen [166].

The concentration of atomic oxygen at the output from an electric-discharge SOG is comparable with that of $O_2(a)$. The removal of $O(^3P)$ from the mixture should lead to the increase in the SOG efficiency due to the exclusion of loss channel (2.38). Recently the authors of [38] have managed to increase the content of $O_2(a)$ at the output of a radio-frequency discharge (81 MHz) from 10 %–12 % to 16% by covering the walls of the discharge chamber with mercury oxide (to remove excessive oxygen atoms). In this case, the oxygen pressure was increased by a factor of five compared to that achieved in earlier papers [22, 32].

3.2 Quantum yield of $O_2(a)$ in reactions of $O(^1D)$ with N_2O and of $O(^3P, ^1D)$ with NO_2

The UV photolysis of N_2O is widely used for the production of electronically excited $O(^1D)$ atoms [process (2.3)]. The reaction of the photofragment $O(^1D)$ with N_2O proceeds via three channels: (2.4), (2.5), and (2.6). These reactions have been extensively studied because one of the products (the NO molecule) is involved in the destruction of the ozone layer [167]. The spin conservation law and *ab initio* calculations [168] predict the production of singlet oxygen $O_2(a)$ in reaction (2.5).

The PLP of N_2O–Ar mixture at 193 nm was used to observe $O_2(a)$ production from reaction (2.5) [169]. The quantum yield of $O(^1D)$ atoms in the photolysis of N_2O at a wavelength of 193 nm is 0.995 [157]. The emission of oxygen at the a–X transition was selected with a 1268-nm interference filter and detected with an ADC 403HS germanium photodetector with a response time of ~ 1 μs, which was cooled with liquid nitrogen. After irradiation by a laser pulse, long-lived fluorescence with a maximum at ~ 1268 nm was observed, which confirms the production of $O_2(a)$. Curve I_{N_2O} in Fig. 9 shows the time dependence of emission at 1268 nm during the photolysis of the N_2O–Ar mixture ($P_{N_2O} = 207$ Torr, $P_{Ar} = 407$ Torr). The rapid decay of the emission intensity (for 0.2 ms) at the initial part of the curve is determined by the emission of electronically excited NO_2^* molecules produced in process (2.39). The NO molecules are produced in reaction (2.4), and $O(^3P)$ atoms – in reaction (2.6). Note that the emission intensity of NO_2^* molecule at extremely low concentrations can be comparable with the emission intensity of $O_2(a)$ due to the huge difference in the radiative lifetimes of NO_2^* and $O_2(a)$ (by 10^8 times). The intensity I_{N_2O} is almost constant for $t > 0.3$ ms, and its value was used to determine the concentration of $O_2(a)$ molecules produced in process (2.5).

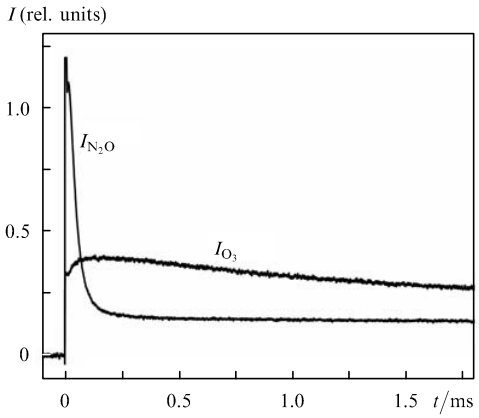


Figure 9. Time dependences of the emission intensity of $O_2(a)$ at ~ 1268 nm upon photolysis of the $O_3 - N_2$ (I_{O_3}) mixture for $P_{N_2} = 773.7$ Torr, $P_{O_3} = 1.3$ Torr and of the $N_2O - Ar$ (I_{N_2O}) mixture for $P_{N_2O} = 207$ Torr and $P_{Ar} = 407$ Torr [169].

The equipment for measuring the $O_2(a)$ concentration was calibrated by using the PLP of the $O_3 - N_2$ mixture at a wavelength of 248 nm. The quantum yield of singlet oxygen in process (2.1) $\eta_{\Delta,2.1} = [O_2(a)]/[O_2]$ is close to 0.9 [155]. The trace labelled I_{O_3} in Fig. 9 is the typical time dependence of the emission intensity of $O_2(a)$ after the PLP of ozone. A signal immediately after photolysis ($t = 0$) is proportional to the concentration of $O_2(a)$ molecules produced during the action of the photolysis pulse. A small increase in the signal intensity at the initial part of the curve (0–0.2 ms) is caused by the additional production of $O_2(a)$ during the three-body recombination of oxygen atoms [72]. The intensity decay is mainly determined by the quenching of $O_2(a)$ by O_3 molecules. The number of $O_2(a)$ molecules produced upon the photolysis of O_3 is determined by the expression

$$N_\Delta^{O_3} = \frac{\Delta E_{248}\lambda_{248}}{hc}\,\eta_{\Delta,2.1},$$

where ΔE is the fraction of the laser pulse energy absorbed in the photolysis volume.

The number of $O_2(a)$ molecules produced in process (2.5) can be determined from the expression

$$N_\Delta^{N_2O} = \frac{\Delta E_{193}\lambda_{193}}{hc}\,\gamma_{2.5}\eta_{\Delta,2.5},$$

where $\gamma_{2.5} = K_{2.5}/(K_{2.4} + K_{2.5} + K_{2.6})$ and $\eta_{\Delta,2.5}$ is the quantum yield of $O_2(a)$ in reaction (2.5). Taking into account that the emission intensity at a wavelength of 1268 nm is directly proportional to the concentration of $O_2(a)$, we can easily obtain from the relation $N_\Delta^{O_3}/N_\Delta^{N_2O} = I_{O_3}/I_{N_2O}$ the required quantum yield

$$\eta_{\Delta,2.5} = \frac{I_{N_2O}}{I_{O_3}}\,\frac{\Delta E_{248}\lambda_{248}}{\Delta E_{193}\lambda_{193}}\,\frac{\eta_{\Delta 2.5}}{\gamma_{2.5}} = 3.08\,\frac{I_{N_2O}}{I_{O_3}}\,\frac{\Delta E_{248}}{\Delta E_{193}}.$$

Table 3 presents the data for measuring the quantum yield of $O_2(a)$ in process (2.5). The processing of the data showed that the quantum yield is $\eta_{\Delta,2.5} = 1.00 \pm 0.12$.

Table 3. Data for determining the quantum yield $\eta_{\Delta,2.5}$ of $O_2(a)$ in process (2.5) [169].

I_{N_2O}/mV	I_{O_3}/mV	ΔE_{193}/mJ	ΔE_{248}/mJ	$\eta_{\Delta,2.5}$
0.15	0.35	14.4	11.2	1.03
0.15	0.35	15.8	11.2	0.94
0.14	0.33	14.2	11.2	1.03
0.14	0.51	16	18.4	0.97
0.11	0.33	11	11.2	1.05
0.1	0.3	9.2	8.4	0.94
0.14	0.38	12.6	12.6	1.13
0.17	0.54	16.8	16.8	0.97
0.072	0.3	6.4	8.4	0.97
0.14	0.56	12.6	15.6	0.95

By simulating the kinetics of reactions in the post-discharge zone, the authors of paper [84] concluded that the increase in the concentration of I^* after the addition of NO_2 cannot be explained only by the removal of excessive O atoms from the mixture. To obtain agreement with the concentrations of I^* observed in experiments, it was necessary to introduce to the model the additional source of $O_2(a)$. The authors assumed that $O_2(a)$ was produced in the process $O(^3P) + NO_2 \rightarrow O_2(a) + NO$. In [169], the PLP of the Ar–NO_2 mixture at a wavelength of 193 nm was used to determine the quantum yield of $O_2(a)$ in reaction (2.28). During the photolysis of NO_2 at 193 nm, the $O(^3P)$ and $O(^1D)$ atoms are produced with the quantum yields 0.45 and 0.55, respectively [170]. These yields were used to

determine the yields of $O_2(a)$ in reaction (2.28) and in the reaction of $O(^1D)$ with NO_2. The examine the production of $O_2(a)$ only from process (2.28), nitrogen was added to the gas mixture in order to convert $O(^1D)$ to the $O(^3P)$ ground state. Experiments performed in a broad range of parameters have not revealed the luminescence of $O_2(a)$ at 1268 nm. The sensitivity of the equipment was sufficient for detecting this emission for the quantum yield of $O_2(a)$ in process (2.28) exceeding 10 %.

3.3 Quenching of I^* by $O(^3P)$, O_3, NO_2, N_2O_4, and N_2O molecules

Because process (2.12) is one of the fastest deactivation processes in EOILs and POILs, it is very important to determine accurately the value of $K_{2.12}$. In this connection it is reasonable to use several methods for measuring this rate constant. In [169], the kinetics of the reaction of I^* with $O(^3P)$ was studied by using the PLP of the $N_2O - I_2 - CO_2 - N_2$ mixture. The production of the required concentration of oxygen atoms by means of the N_2O photolysis is an important factor in experiments on measuring the rate of quenching of I^* atoms by atomic oxygen. The experimental conditions in [169] were chosen so that the rate of quenching of I^* by $O(^3P)$ atoms dominated over the rates of quenching by I_2, N_2O, IO, etc. Molecular iodine is a strong quencher of I^* (3.8×10^{-11} cm^3 s^{-1} [11]). The rate of quenching of I^* by an IO radical is unknown. The concentration of oxygen atoms generated in the photolysis of N_2O should be considerably higher than the initial concentration of I_2. In this case, molecules I_2 and IO will almost completely react with oxygen in processes (2.19) and (2.20), and the excess of oxygen atoms quenching I^* should remain, which requires the use of low initial concentrations of I_2, high N_2O pressures, and high-energy laser pulses.

The time dependences of concentrations of I_2 and IO were measured by the LIF method [169].

The time dependences of concentrations of I_2 and IO were detected to find the regimes providing the rapid exhaustion of these components. Moreover, the time profiles of the I_2 concentration were used for determining the concentration of oxygen atoms. Figure 10 shows typical time profiles of the I_2 concentration. Experiments were performed at the partial gas pressures $P_{N_2O} = 16.7$, $P_{CO_2} = 16.7$, and $P_{I_2} = 0.0038$ Torr. Taking into account that the rate constant of process (2.19) is known quite accurately, the time dependences of the I_2 concentration were used to determine the concentration of $O(^3P)$ atoms. Thus, the initial concentration of $O(^3P)$ atoms was found by fitting experimental data by the calculated concentration of I_2.

Experiments were performed when the concentration $[O(^3P)]$ considerably exceeded the concentration of molecular iodine. Molecules I_2 and IO were completely spent in chemical reactions for the time $t \leqslant 100$ μs. Figure 11 shows typical time profiles of the emission intensity at the $I^* \rightarrow I$ transition. The dependences of this type are typical for cases when emitting particles are produced in secondary processes. The increase in the emission intensity at the initial parts of the curves is caused by the production of iodine atoms in chemical reactions (2.19) and (2.20) followed by their excitation during energy exchange (2.7). The decrease in the emission intensity of I^* in Fig. 11 is caused by the deactivation of iodine atoms in process (2.12). The numerical simulation of photochemical processes was used to analyse the time profiles of the I^* concentration. The best agreement between calculations and experiments was achieved for $K_{2.12} = 1.2 \times 10^{-11}$ cm^{3}s^{-1} [169].

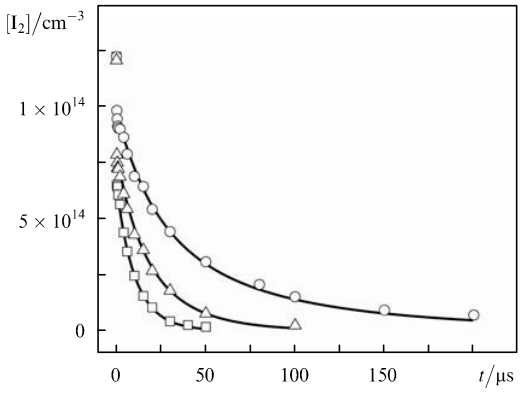


Figure 10. Time profiles of the concentration of I_2 after PLP of the $N_2O - I_2 - CO_2 - Ar$ mixture at a wavelength of 193 nm for $P_{tot} = 50$ Torr, $P_{CO_2} = 16.7$ Torr, $P_{N_2O} = 16.7$ Torr, $P_{I_2} = 3.8$ mTorr and pulse energy densities 31.5 (□), 18 (△) and 10 mJ cm^{-2} (○). The solid curves are the concentrations of I_2 calculated for experimental conditions [169].

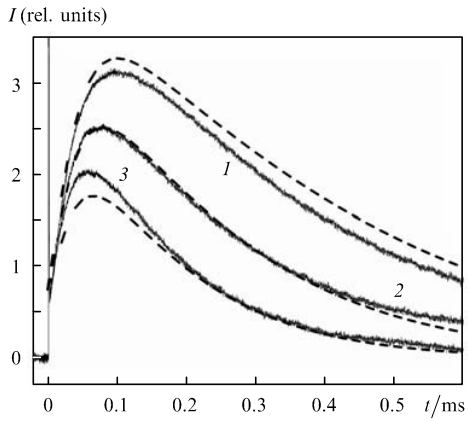


Figure 11. Time dependences of the emission intensity of I^* after PLP of the $N_2O - I_2 - CO_2 - Ar$ mixture at a wavelength of 193 nm for $P_{tot} = 50$ Torr, $P_{N_2O} = 16.7$ Torr, $P_{I_2} = 4.1$ mTorr, $E_{las} = 31.5$ mJ cm^{-2} and $P_{CO_2} = 8.3$ (*1*), 16.7 (*2*) and 33.3 Torr (*3*); The dashed curves are the relative concentrations of I^* calculated for $K_{2.12} = 1.2 \times 10^{11}$ cm^3 s^{-1} [169].

Oxygen atoms are also involved in the production of ozone in processes (2.36) and (2.37). Ozone reacts both with I^* and I in processes (2.17) and (2.18). One of the products of these reactions is a short-lived IO radical. The process IO + IO leads to the production of IO_2 and I_2O_2 molecules [171], which is undesirable because in this case iodine atoms are removed from the system, while reaction products IO, IO_2, and I_2O_2 can quench I^* and $O_2(a)$.

The reaction of atomic iodine with ozone is one of the loss channels of O_3 in the atmosphere [167]. The rate constant of process (2.18) was measured by several methods. These measurements were analysed in [157], and the rate constant of this process equal to 1.2×10^{-12}cm^3 s^{-1} was recommended.

The authors of paper [172] measured the rate constant of process (2.17) by using the flashlamp photolysis of the CF_6I-O_3 mixture to produce excited iodine atoms I^*. The rate constant of quenching of I^* by ozone was measured to be 1.1×10^{-11} cm^3 s^{-1}. The broadband flashlamp photolysis caused the photodissociation of not only CF_3I but also of a great amount of O_3. The photolysis of ozone produces both $O(^3P)$ atoms and O_2 molecules, which efficiently quench I^* in processes (2.8) and (2.12). The products of the ozone photolysis accelerated the quenching rate of I^*, which resulted in the overstating of the rate constant of process (2.17).

The rate constant of I^* quenching by O_3 molecules was also measured in [158] by two different methods. In the first case, the PLP of the $I_2 - O_3$ mixture at 485 nm was used. In the second case, the kinetics of deactivation of I^* by $O(^3P)$ atoms and O_3 molecules was studied by using the PLP of the $I_2 - O_3 - N_2$ mixture by radiation at 248 or 266 nm. The photolysis of I_2 by radiation at 485 nm (the iodine absorption cross section at this wavelength is 1.52×10^{-18} cm^2 [157]) was used to produce I^* atoms:

$$I_2(X) + h\nu\,(485\text{ nm}) \rightarrow I_2(B) \rightarrow I^* + I,$$

$$I_2(X) + h\nu\,(485\text{ nm}) \rightarrow I_2(^1\Pi_{1u}) \rightarrow I + I.$$

The relative yield $\phi = [I^*]/([I^*] + [I])$ of excited I^* atoms in this process lies in the range 0.23–0.3 [64, 173]. The ozone absorption cross section at 485 nm is comparatively low (7×10^{-22} cm^2) [157], and, therefore, the fraction of O_3 subjected to photolysis was insignificant.

The time dependences of the emission intensity of atomic iodine at the $I^* \rightarrow I$ transition were used to determine the rate of quenching of I^* by O_3 molecules. The rate constant $K_{2.17}$ of process (2.17) obtained in this way was 2.6×10^{-12} cm^3 s^{-1} [158]. The fraction of residual O_2 in the ozone flow was not controlled, and therefore this value most likely corresponds to the upper bound of the constant $K_{2.17}$.

The main products of the photolysis of ozone at the wavelengths of 248 or 266 nm are $O(^1D)$ and $O_2(a)$. Electronically excited atomic iodine is produced in the sequence of reactions (2.24), (2.19), (2.20), and (2.7). The time dependences of luminescence of I^* were similar to those presented in Fig. 11. The decay of the emission intensity is caused by the deactivation of I^* in collisions with $O(^3P)$, O_3, and I_2. The time dependences of the emission intensity of I^* were obtained in a broad range of compositions of the medium and energies of the laser photolysis pulse. The rate constants of processes (2.12) and (2.17) were found from the numerical analysis of time dependences of luminescence of I^* [158]. The values of rate constants of processes used in calculations are presented in Table 2. The best agreement between calculations and experiments was achieved for $K_{2.12} = 1.2 \times 10^{-11}$ cm^3 s^{-1} and $K_{2.17} = 1.8 \times 10^{-12}$ cm^3 s^{-1}. The value of $K_{2.17}$ found by this method should be considered more accurate than that measured by the first method because the results of calculations were insensitive to the initial relative oxygen content in the $I_2 - O_3 - N_2$ mixture up to $[O_2]/[O_3] \leqslant 10\,\%$. The difference between the rate constants $K_{2.17}$ found by two different methods [158] (2.6×10^{-12} and 1.8×10^{-12} cm^3 s^{-1}) shows that the residual content of oxygen in ozone prepared for experiments is $\sim 3\,\%$. The rate constant of quenching of I^* by $O(^3P)$ atoms well agrees with its value measured in experiments on the UV photolysis of the $N_2O - I_2 - CO_2 - N_2$ mixture [169].

The addition of NO_2 to the mixture at the output of an electric-discharge SOG reduces the relaxation rate of the stored energy [33]. The optimal content of added NO_2 should depend on the quenching rate of I^* in processes (2.13) and (2.14). A N_2O_4 dimer always accompanies NO_2. The rate constant of reaction (2.13) was first estimated in paper [174]. The excited atomic iodine was produced by the PLP of the $CF_3I - NO_2 - N_2O_4$ mixture at a wavelength of 248 nm. This rate constant was estimated to be 8.5×10^{-14} cm^3 s^{-1} at room temperature by neglecting the influence of a N_2O_4 dimer and some other secondary photochemical processes.

The rate constants of processes (2.13)–(2.15) were measured in [159] at gas temperatures from 293 to 380 K. The measurements of these rate constants at high temperatures were performed by several reasons. First, the gas temperature in the post-discharge zone is relatively high (more than 400 K), and, therefore, it is important to find the temperature dependences of the rate constants. Second, the content of dimers in the mixture strongly decreases with increasing temperature, and to exclude the influence of N_2O_4 on the measurement of the rate constant of process (2.13), experiments were performed at temperatures above room temperature.

The rate constants of quenching of I^* by nitrogen oxides were measured using the PLP of the $CF_3I - NO_2 - N_2O_4$ (or N_2O) mixture at a wavelength of 248 nm [159]; I^* was produced by the photolysis of CF_3I in process (2.2). The ratio of the quantum yields of the photodissociation channels of CF_3I was 0.89 : 0.11 [156]. The study of quenching of I^* by NO_2 molecules was complicated by the influence of secondary reactions. One of the products of NO_2 photolysis is atomic oxygen, which rapidly transforms to molecular oxygen in process (2.28). The contribution of molecular oxygen to the quenching rate of I^* was of the same order of magnitude as that of the molecule under study. To exclude the influence of O_2 on the deactivation rate of I^*, measurements were performed at different energy densities of the laser photolysis pulse (3.5–12.6 mJ cm^{-2}) at a fixed pressure of NO_2. Then, the quenching rates R were extrapolated by a linear function to $E = 0$. The quenching rate $R_{E=0}$ is equal to the sum of rates of quenching rates by NO_2 molecules (R_{NO_2}) and impurity molecules I_2 (R_{I_2}). The quenching rate R_{NO_2} was found from the relation $R_{NO_2} = R_{E=0} - R_{I_2}$. The value of R_{I_2} was measured for $P_{NO_2} = 0$.

The influence of the secondary products of the CF_3I photolysis on the measurement of the rate constants was considerably weaker than that of the secondary products of the NO_2 photodissociation. Based on the analysis of the dependences of deactivation rates of I^* on the partial pressure of CF_3I, the rate constant of deactivation of I^* by one of the products of the reaction of CF_3 with NO_2 was estimated as 2×10^{-11} cm^3 s^{-1}. It is most likely that this product is the CF_2O molecule [175].

The rate of deactivation of I^* by NO_2 molecules at room temperature was not measured because the concentration of N_2O_4 dimers at this temperature is relatively high, and the decay of emission of atomic iodine was mainly determined by quenching by the dimer. At gas temperatures $T \geqslant 320$ K, the influence of N_2O_4 can be neglected. The rate constant of

quenching of I^* by NO_2 molecules is independent of temperature in the interval from 320 to 381 K, its average value being 2.9×10^{-15} cm^3 s^{-1} [159].

At room temperature and $P_0 = P_{NO_2} + P_{N_2O_4} \geqslant 2$ Torr, the quenching of I^* by N_2O_4 molecules is more efficient than that by NO_2 molecules. The analysis of dependences of relaxation rates of I^* on the total pressure P_0 showed that the rate constant of the process $I^* + N_2O_4 \rightarrow$ products can be estimated as 3.5×10^{-13} cm^3 s^{-1} [159]. This is almost two orders of magnitude higher than the rate constant of the process $I^* + NO_2 \rightarrow I + NO_2$. It was found in the same paper that the rate constant of quenching of I^* by N_2O molecules is independent of temperature in the interval 293–378 K and is equal to 1.4×10^{-15} cm^3 s^{-1}. This value well agrees with the value obtained earlier [176].

4. Conclusions

The standard kinetic package for a COIL was proposed more than a decade ago [11]. Recently, new kinetic data were obtained and some mechanisms of the production of electronically and vibrationally excited molecules O_2 and I_2, which can play an important role in the dissociation of iodine, were reconsidered. The multichannel model of I_2 dissociation involving vibrationally excited molecules $O_2(a, v)$ and $I_2(X, v)$ and the lower excited electronic states of $I_2(A', A)$ proposed recently [124] provides the dissociation rate of iodine observed in real mixing devices used in OILs. At present, it is impossible to state certainly that dissociation proceeds according to the proposed scheme, but its successful testing additionally stimulates further investigations and indicates the direction of solving this long-standing problem. The further development of the proposed kinetic dissociation scheme of iodine requires the measurement of the rate constants of processes (95)–(103) and the distributions of energies released in processes (1), (3), (5), (9), (33), (44), and (45) among products.

At present an OIL in which $O_2(a)$ is produced in an electric-discharge SOG attracts great interest. The advantages of the electric-discharge generator of $O_2(a)$ is nontoxicity of initial gas components O_2, He, and Ar and also the possibility of the repeated use of reagents in a closed loop. A low oxygen pressure and a relatively small η_Δ (15 %–20 %) at the output of the electric-discharge SOG cannot provide the acceptable gain in the active medium of EOILs [33]. An increase in the oxygen pressure is accompanied by the increase in the quenching rate of $O_2(a)$ [38]. The quenching mechanism of $O_2(a)$ in the presence of oxygen atoms and molecules is not clear completely. The two possible deactivation channels of $O_2(a)$ were proposed. In the first channel, singlet oxygen is quenched in three-body process (2.38) with the formation of electronically excited intermediate complex $(O_3)^*$ [38]. In the second channel, singlet oxygen can be quenched in collisions with vibrationally excited ozone molecules $O_3(v)$ [166]. Molecules $O_3(v)$ in the $O-O_2$ mixture are produced during the recombination of oxygen atoms in the process $O + O_2 + M \rightarrow O_3(v) + M$. The understanding of the quenching mechanism of $O_2(a)$ in the presence of oxygen atoms and molecules will allow one to determine the upper attainable pressure limit for O_2 in the electric-discharge SOG and will favour the search for the ways to improve the efficiency of the electric-discharge SOG whose potential has not been used completely so far. In recent paper [177], the record singlet oxygen yield $\eta_\Delta \approx 45$ % was achieved in the electric-discharge SOG. The authors of this paper found the efficient channel of the $O_2(a)$ production during the heterogeneous recombination of oxygen atoms.

Note that the processes of production of $O_2(a)$ molecules in reaction (2.5) and their quenching in process (2.38) can be of interest for atmospheric physics. The emission of oxygen at the IR $O_2(a-X)$ transition is one of the most intense emissions of the earth atmosphere [178]. Under certain conditions, these processes can noticeably affect the balance of $O_2(a)$ in the atmospheres of planets. The UV photolysis of N_2O is a convenient method for producing singlet oxygen in laboratory conditions for studying the kinetics of processes involving $O_2(a)$, as was first demonstrated in [169] by measuring the rate constant of process (2.12).

5. References

1. Kasper J.V.V., Pimentel G.C. *Appl. Phys. Lett.*, **5**, 231 (1964).
2. Devis C.C., Pirkle R.J., McFarlane R.A., Wolga G.J. *IEEE J. Quantum Electron.*, **QE-12**, 334 (1976).
3. Ershov L.S., Zalesskii V.Yu., Sokolov I.I. *Kvantovaya Elektron.*, **5**, 863 (1978) [*Sov. J. Quantum Electron.*, **8**, 494 (1978)].
4. Alekseev A.B., Pravilov A.M., Sidorov I.I., Skorokhodov V.A. *Kvantovaya Elektron.*, **14**, 2421 (1987) [*Sov. J. Quantum Electron.*, **17**, 1539 (1987)].
5. Brederlov G., Fill E., Vitte K. *Moshchnyi iodnyi lazer* (High-power Iodine Laser) (Moscow: Energoatomizdat, 1985).
6. Hola K., Kompa K., in *Khimicheskie lazery* (Chemical Lasers) (Moscow: Mir, 1980) p. 757.
7. Zalesskii V.Yu., Krupennikova T.I. *Opt. Spektrosk.*, **30**, 813 (1971).
8. McDermott W.E., Pchelkin N.R., Benard D.J., Bousek R.R. *Appl. Phys. Lett.*, **32**, 469 (1978).
9. Henshaw T.L., Manke II G.C., Madden T.J., Berman M.R., Hager G.D. *Chem. Phys. Lett.*, **325**, 537 (2000).
10. Manke II G.C., Cooper C.B., Dass S.C., Madden T.J., Hager G.D. *Proc. SPIE Int. Soc. Opt. Eng.*, **5448**, 251 (2004).
11. Perram G.P. *Int. J. Chem. Kinet.*, **27**, 817 (1995).
12. Ray A.J., Coombe R.D. *J. Phys. Chem.*, **97**, 3475 (1993).
13. Henshaw T.L., Herrera S.D., Schlie A.V. *J. Phys. Chem.*, **102**, 6239 (1998).
14. Didyukov A.I., Krasnoshchekov Yu.I., Kulagin Yu.A., Morozov V.A., Reshetnyak S.A., Shelepin L.A. *Kvantovaya Elektron.*, **9**, 645 (1982) [*Sov. J. Quantum Electron.*, **12**, 399 (1982)].
15. Shinkarenko N.V., Aleskovskii V.B. *Usp. Khim.*, **50**, 406 (1981).
16. Frimer A.A. *Singlet O2* (Boca Raton, Florida: CRC Press Inc., 1985) Vol. 1, p. 81.
17. Koop G., Hartlove J., Clendening C., et al. *AIAA-2000-2421* (Denver, CO, June 19–22, 2000).
18. Slanger T.G. *Science*, **265**, 1817 (1994).
19. Atkinson R., Baulch D.L., Cox R.A., Hampson R.F., Kerr J.A., Rossi M.J., Troe J. *J. Phys. Chem. Ref. Data*, **29**, 167 (2000).
20. Heaven M.C. *Adv. Ser. Phys. Chem.*, **11**, 138 (2001).
21. Napartovich A.P., Deryugin A.A., Kochetov I.V. *J. Phys. D: Appl. Phys.*, **34**, 1827 (2001).
22. Vasiljeva A.N., Klopovskiy K.S., Kovalev A.S., Lopaev D.V., Mankelevich Y.A., Popov N.A., Rakhimov A.T., Rakhimova T.V. *J. Phys. D: Appl. Phys.*, **37**, 2455 (2004).
23. Starik A.M., Lukhovitskii B.I., Titova N.S. *Fiz. Goren. Vzryv.*, **44**, 3 (2008).
24. Hatz S., Poulsen L., Ogilby P.R. *Photochem. Photobiol.*, **84**, 1284 (2008).
25. Niedre M.J., Secord A.J., Patterson M.S., Wilson B.C. *Cancer Research*, **63**, 7986 (2003).
26. Arnold S.J., Finlayson N., Ogryzlo E.A. *J. Chem. Phys.*, **44**, 2529 (1966).

27. Derwent R.G., Kearns D.R., Thrush B.A. *Chem. Phys. Lett.*, **6**, 115 (1970).
28. Derwent R.G., Thrush B.A. *J. Chem. Soc. Far. Trans.*, **68**, 720 (1972).
29. Derwent R.G., Thrush B.A. *Far. Discuss. Chem. Soc.*, **53**, 162 (1972).
30. Zolotarev V.A., Ishkov D.V., Podmar'kov Yu.P., Frolov M.P., Yuryshev N.N. *Kvantovaya Elektron.*, **18**, 912 (1991) [*Sov. J. Quantum Electron.*, **21**, 826 (1991)].
31. Ionin A.A., Klimachev Yu.M., Kotkov A.A., Kochetov I.V., Napartovich A.P., Seleznev L.V., Sinitsyn D.V., Hager G.D. *J. Phys. D: Appl. Phys.*, **36**, 982 (2003).
32. Braginsky O.V., Vasiljeva A.N., Klopovskiy K.S., Kovalev A.S., Lopaev D.V., Proshina O.V., Rakhimov A.T., Rakhimova T.V. *J. Phys. D: Appl. Phys.*, **38**, 3609 (2005).
33. Carroll D.L., Verdeyen J.T., King D.M., Zimmerman J.W., Laystrom J.K., Woodard B.S., Benavides G.F., Kittell K.W., Solomon W.C. *IEEE J. Quantum Electron.*, **41**, 213 (2005).
34. Carroll D.L., Verdeyen J.T., King D.M., et al. *Appl. Phys. Lett.*, **86**, 111104 (2005).
35. Rawlins W.T., Lee S., Kessler W.J., Davis S.J. *App. Phys. Lett.*, **86**, 051105 (2005).
36. Carroll D.L., Verdeyen J.T., King D.M., et al. *IEEE J. Quantum Electron.*, **41**, 1309 (2005).
37. Proshina O.V., Rakhimova T.V., Braginsky O.V., Kovalev A.S., Lopaev D.V., Mankelevich Yu.A., Rakhimov A.T., Vasilieva A.N. *J. Phys. D: Appl. Phys.*, **39**, 5191 (2006).
38. Braginsky O.V., Kovalev A.S., Lopaev D.V., Mankelevich Yu.A., Proshina O.V., Rakhimova T.V., Rakhimov A.T., Vasilieva A.N. *J. Phys. D: Appl. Phys.*, **39**, 5183 (2006).
39. Ionin A.A., Napartovich A.P., Yuryshev N.N. *Proc. SPIE Int. Soc. Opt. Eng.*, **4631**, 284 (2002).
40. Hicks A., Tirupathi S., Jiang N., Utkin Yu., Lempert W.R., Rich J.W., Adamovich I.V. *J. Phys. D: Appl. Phys.*, **40**, 1408 (2007).
41. Savin Yu.V., Goryachev L.V., Adamenkov Yu.A., et al. *J. Phys. D: Appl. Phys.*, **37**, 3121 (2004).
42. Azyazov V.N., Zagidullin M.V., Nikolaev V.D., Ufimtsev N.I., *Zh. Fiz. Khim.*, **72**, 1850 (1998) [*Russian J. Phys. Chem.*, **72**, 1681 (1990)].
43. Pritt A.T., Coombe R.D., Pilipovich D., Wagner R.I., Benard D., Dymec C. *Appl. Phys. Lett.*, **31**, 745 (1977).
44. Basov N.G., Zagidullin M.V., Igohin V.I., Katulin V.A., Kupriyanov N.L. *Trudy FIAN*, **171**, 30 (1986).
45. Storch D.J., Dymec C.J., Davis L.P. *J. Amer. Chem. Soc.*, **105**, 1765 (1983).
46. Yuryshev N.N. *Kvantovaya Elektron.*, **23**, 583 (1996) [*Quantum Electron.*, **26**, 567 (1996)].
47. Zagidillin M.V., Nikolaev V.D. *Izv. Ross. Akad. Nauk, Ser. Fiz.*, **63**, 1901 (1999).
48. Barmashenko B.D., Rosenwaks S. *J. Appl. Phys.*, **73**, 1598 (1993).
49. Azyazov V.N., Kupriyanov N.L. *Trudy FIAN*, **194**, 148 (1989).
50. Azyazov V.N., Kupriyanov N.L. *J. Russian Laser Research*, **15**, 243 (1994).
51. Basov N.G., Vagin N.P., Kryukov P.G., Nurligareev D.Kh., Pazyuk V.S., Yuryhev N.N. *Kvantovaya Elektron.*, **11**, 1893 (1984) [*Sov. J. Quantum Electron.*, **14**, 1275 (1984)].
52. Rybalkin V., Katz A., Waichman K., Vingurt D., Dahan Z., Barmashenko B.D., Rosenwaks S. *Appl. Phys. Lett.*, **89**, 021115 (2006).
53. Fisk G.A., Hays G.N. *J. Chem. Phys.*, **77**, 4965 (1982).
54. Didyukov A.I., Kulagin Yu.A., Shelepin L.A., Yarygina V.N. *Kvantovaya Elektron.*, **16**, 892 (1989) [*Sov. J. Quantum Electron.*, **19**, 578 (1989)].
55. Lilenfeld H.V. *Final Report of McDonnell Douglas Research Laboratories AFWL-TR-83-1* (May, 1983).
56. Marter T., Heaven M.C., Plummer D. *Chem. Phys. Lett.*, **260**, 201 (1996).
57. Burde D.H., McFarlane R.A. *J. Chem. Phys.*, **64**, 1850 (1976).
58. Derwent R.G., Thrush B.A. *Chem. Phys. Lett.*, **9**, 591 (1971).
59. Burrows M.D. *J. Chem. Phys.*, **81**, 3546 (1984).
60. Young A.T., Houston P.L. *J. Chem. Phys.*, **78**, 2317 (1983).
61. Burde D.H., Yang T.T., McFarlane R.A. *Chem. Phys. Lett.*, **205**, 69 (1993).
62. Kaledin A.L., Heaven M.C., Morokuma K. *J. Chem. Phys.*, **114**, 215 (2001).
63. Heidner R.F., Gardner C.E., El-Sayed T.M., Segal G.I., Kasper J.V.V. *J. Chem. Phys.*, **74**, 5618 (1981).
64. Cline J.I., Leone S.R. *J. Phys. Chem.*, **95**, 2917 (1991).
65. Lilenfeld H.V., Whitefield P.D., Bradburn G.R. *J. Phys. Chem.*, **88**, 6158 (1984).
66. Lilenfeld H.V., Carr P.A.G., Hovis F.E. *J. Chem. Phys.*, **81**, 5730 (1984).
67. Aviles R.G., Muller D.F., Houston P.L. *Appl. Phys. Lett.*, **37**, 358 (1980).
68. Heaven M.C., Komissarov A.V., Goncharov V. *Proc. SPIE Int. Soc. Opt. Eng.*, **4631**, 13 (2002).
69. Han J., Komissarov A.V., Tinney S.P., Heaven M.C. *Proc. SPIE Int. Soc. Opt. Eng.*, **5777**, 198 (2005).
70. Heidner R.F., Gardner C.E., Segal G.I., El-Sayed T.M. *J. Phys. Chem.*, **87**, 2348 (1983).
71. Komissarov A.V., Heaven M.C. *J. Phys. Chem. A*, **107**, 10527 (2003).
72. Palla A.D., Carroll D.L., Verdeyen J.T., Solomon W.C. *AIAA-2005-4919* (Toronto, June 6–9, 2005).
73. Vagin N.P., Zolotarev V.A., Kryukov P.G., Pazyuk V.S., Podmar'kov Yu.P., Frolov M.P., Yuryshev N.N. *Kvantovaya Elektron.*, **18**, 33 (1991) [*Sov. J. Quantum Electron.*, **21**, 28 (1991)].
74. Muller D.F., Young R.H., Houston P.L., Wiesenfeld J.R. *Appl. Phys. Lett.*, **38**, 404 (1981).
75. Heaven M.C., Han J., Davis S.J., Lee S. *Proc. SPIE Int. Soc. Opt. Eng.*, **5334**, 53 (2004).
76. Biryukov A.S., Shcheglov V.A. *Kvantovaya Elektron.*, **13**, 510 (1986) [*Sov. J. Quantum Electron.*, **16**, 333 (1986)].
77. Antonov I.O., Azyazov V.N., Ufimtsev N.I. *J. Chem. Phys.*, **119**, 10638 (2003).
78. Antonov I.O., Azyazov V.N., Pichugin S.Yu., Ufimtsev N.I. *Chem. Phys. Lett.*, **376**, 168 (2003).
79. Azyazov V.N., Safonov V.S., Ufimtsev N.I. *Kvantovaya Elektron.*, **30**, 687 (2000) [*Quantum Electron.*, **30**, 687 (2000).
80. Azyazov V.N. Antonov I.O., Pichugin S.Yu., Safonov V.S., Svistun M.I., Ufimtsev N.I. *Kvantovaya Elektron.*, **33**, 811 (2003) [*Quantum Electron.*, **33**, 811 (2003)].
81. Zagidullin M.V., Igoshin V.I., Katulin V.A., Kupriyanov N.L., *Kvantovaya Elektron.*, **11**, 382 (1984) [*Sov. J. Quantum Electron.*, **14**, 259 (1984)].
82. Vagin N.P., Ionin A.A. Klimachev Yu.M., et al. *Kvantovaya Elektron.*, **34**, 865 (2004) [*Quantum Electron.*, **34**, 865 (2004)].
83. Azyazov V.N. *Kvantovaya Elektron.*, **21**, 25 (1994) [*Quantum Electron.*, **24**, 23 (1994)].
84. Zimmerman J.W., King D.M., Palla A.D., et al. *Proc. SPIE Int. Soc. Opt. Eng.*, **6261**, 62611R (2006).
85. Hays G.N., Fisk G.A. *IEEE J. Quantum Electron.*, **QE-17**, 1823 (1981).
86. Byteva N.M., Chernikov V.S. *Zh. Fiz. Khim.*, **68**, 1208 (1989).
87. Rodgers M.A., Snowden P.T. *J. Am. Chem. Soc.*, **104**, 5541 (1982).
88. Benard D.J., McDermott W.E., Pchelkin N.R., Bousek R.R. *Appl. Phys. Lett.*, **34**, 40 (1979).
89. Bachar J., Rosenwaks S. *Appl. Phys. Lett.*, **41**, 16 (1982).
90. Watanabe K., Kashiwabara S., Sawai K., Toshima S., Fujimoto R. *J.Appl. Phys.*, **54**, 1228 (1983).
91. Vagin N.P., Konoshenko A.F., Kryukov P.G., Nurligareev D.Kh., Pazyuk V.S., Tomashev V.N., Yuryshev N.N. *Kvantovaya Elektron.*, **11**, 1688 (1984) [*Sov. J. Quantum Electron.*, **14**, 1138 (1984)].
92. Richardson R.J., Wiswall C.E., Carr P.A.G., Hovis F.E., Lilenfeld H.V. *J. Appl. Phys.*, **52**, 4962 (1981).

93. Avizonis P.V., Hasen G., Truesdell K.A. *Proc. SPIE Int. Soc. Opt. Eng.*, **1225**, 448 (1990).
94. Yuryshev N.N. *Kvantovaya Elektron.*, **25**, 410 (1998) [*Quantum Electron.*, **28**, 397 (1998)].
95. Vagin N.P., Kryukov P.G., Nurligareev D.Kh., Pazyuk V.S., Yuryshev N.N. *Kratk. Soobshch. Fiz. FIAN*, (5), 47 (1987).
96. Balan N.F., Gizatullin R.M., Zagidullin M.V., et al. *Kratk. Soobshch. Fiz. FIAN*, (4), 23 (1989).
97. Azyazov V.N., Zagidullin M.V., Nikolaev V.D., Svistun M.I., Khvatov N.A. *Kvantovaya Elektron.*, **24**, 491 (1997) [*Quantum Electron.*, **27**, 477 (1997)].
98. Zagidullin M.V., Nikolaev V.D., Svistun M.I. *Kvantovaya Elektron.*, **21**, 23 (1994) [*Quantum Electron.*, **24**, 21 (1994)].
99. Azyazov V.N., Zagidullin M.V., Nikolaev V.D., Svistun M.I., Khvatov N.A. *Kvantovaya Elektron.*, **22**, 443 (1995) [*Quantum Electron.*, **25**, 418 (1995)].
100. Azyazov V.N., Zagidullin M.V., Nikolaev V.D., Svistun M.I., Khvatov N.A. *Kvantovaya Elektron.*, **21**, 129 (1994) [*Quantum Electron.*, **24**, 120 (1994)].
101. Boreisho A.S., Mal'kov V.M., Savin A.V., Vasil'ev D.N., Evdokimov I.M., Trilis A.V., Strakhov S.Yu. *Kvantovaya Elektron.*, **33**, 307 (2003) [*Quantum Electron.*, **33**, 307 (2003)].
102. Adamenkov A.A., Bakshin V.V., Bogachev A.V., et al. *Kvantovaya Elektron.*, **37**, 601 (2007) [*Quantum Electron.*, **37**, 601 (2007)].
103. Zagidullin M.V., Nikolaev V.D., Svistun M.I., Khvatov N.A. *Kvantovaya Elektron.*, **35**, 907 (2005) [*Quantum Electron.*, **35**, 907 (2005)].
104. Zagidullin M.V., Nikolaev V.D., Svistun M.I., Khvatov N.A. *Kvantovaya Elektron.*, **38**, 794 (2008) [*Quantum Electron.*, **38**, 794 (2008)].
105. Vagin N.N., Pazyuk V.S., Yuryshev N.N. *Kvantovaya Elektron.*, **22**, 776 (1995) [*Quantum Electron.*, **25**, 746 (1995)].
106. Rybalkin V., Katz A., Barmashenko B.D., Rosenwaks S. *Appl. Phys. Lett.*, **85**, 5851 (2004).
107. Davis S.J. *Proc. SPIE Int. Soc. Opt. Eng.*, **4631**, 60 (2002).
108. Jiräsek V., Špalek O., Kodymová J., Čensky M. *Chem. Phys.*, **269**, 167 (2001).
109. Katz A., Dahan Z., Rybalkin V., Waichman K., Barmashenko B.D., Rosenwaks S. *Appl. Phys. Lett.*, **90**, 161122 (2007).
110. Shepelenko A.A., Mikheyev P.A. *Kvantovaya Elektron.*, **33**, 215 (2003) [*Quantum Electron.*, **33**, 215 (2003)].
111. Mikheyev P.A., Shepelenko A.A., Kupryaev N.V. *Teplofiz. Vys. Temp.*, **40**, 34 (2002).
112. Azyazov V.N., Vorob'ev M.V., Voronov A.I., Kupryaev N.V., Mikheyev P.A., Ufimtsev N.I. *Kvantovaya Elektron.*, **39**, 84 (2009) [*Quantum Electron.*, **39**, 84 (2009)].
113. Mikheyev P.A., Azyazov V.N. *J. Appl. Phys.*, **104**, 123111 (2008).
114. Deakin J.J., Husain D. *J. Chem. Soc. Farad. Tran. Pt. II*, **68**, 1603 (1972).
115. Schurath U. *J. Photochem.*, **4**, 215 (1975).
116. Thomas R.G.O., Thrush B.A. *Proc. R. Soc. Lond. A.*, **356**, 295 (1977).
117. Grimley A.J., Houston P.L. *J. Chem. Phys.*, **69**, 2339 (1978).
118. Van Benthem M.H., Davis S.J. *J. Phys.Chem.*, **90**, 902 (1986).
119. Hall G.E., Marinelli W.J., Houston P.L. *J. Phys. Chem.*, **87**, 2153 (1983).
120. Barnault B., Bouvier A.J., Pigache D., Bacis R. *J. Physique IV*, **1**, C7-647 (1991).
121. Browne R.J., Ogryzlo E.A. *Proc. Chem. Soc.*, **117**, 89 (1964).]
122. Azyazov V.N., Nikolaev V.D., Svistun M.I., Ufimtsev N.I. *Kvantovaya Elektron.*, **28**, 212 (1999) [*Quantum Electron.*, **29**, 767 (1999)].
123. Boodaghians R., Borrell P.M., Borrell P., Grant K.R. *J. Chem. Soc. Faraday Trans.*, **78**, 1195 (1982).
124. Azyazov V.N., Pichugin S.Yu., Heaven M.C. *J. Chem. Phys.*, **130**, 104306 (2009).
125. Bloemink H.I., Copeland R.A., Slanger T.G. *J. Chem. Phys.*, **109**, 4237 (1998).
126. Kalogerakis K.S., Copeland R.A., Slanger T.G. *J. Chem. Phys.*, **116**, 4877 (2002).
127. Saran D.V., Pejakovic D.A., Copeland R.A. *AGU Fall Meeting* (San Francisco, 2008, SA31A-1601).
128. Coletti C., Billing G.D. *Chem. Phys. Lett.*, **356**, 14 (2002).
129. Kalogerakis K.S., Copeland R.A., Slanger T.G. *J. Chem. Phys.*, **123**, 044309 (2005).
130. Gordiets B.F., Osipov A.I., Shelepin L.A. *Kineticheskie protsessy v gazakh i molekulyarnye lazery* (Kinetic Processes in Gases and Molecular Lasers) (Moscow: Nauka, 1980).
131. Lopez-Puertas M., Zaragoza G., Kerridge B.J., Taylor F.W. *J. Geophys. Res.*, **100**, 9131 (1995).
132. Huestis D.L. *J. Phys. Chem. A*, **110**, 6638 (2006).
133. Azyazov V.N., Pichugin S.Yu., Safonov V.S., Ufimtsev N.I. *Kvantovaya Elektron.*, **31**, 794 (2001) [*Quantum Electron.*, **31**, 794 (2001)].
134. Azyazov V.N., Antonov I.O., Pichugin S.Yu., Ufimtsev N.I. *Kvantovaya Elektron.*, **34**, 1116 (2004) [*Quantum Electron.*, **34**, 1116 (2004)].
135. Azyazov V.N., Heaven M.C. *AIAA J.*, **44**, 1593 (2006).
136. Azyazov V.N., Mikheyev P.A., Ufimtsev N.I., Fomin E.V., Antonov I.O., Heaven M.C. *J. Appl. Phys.*, **102**, 123108 (2007).
137. Azyazov V.N., Igoshin V.I., Kupriyanov N.L. *Kratk. Soobshch. Fiz. FIAN*, (1, 2), 24 (1992).
138. Lawrence W.G., Van Marter T.A., Nowlin M.L., Heaven M.C. *J. Chem. Phys.*, **106**, 127 (1997).
139. Azyazov V.N., Pichugin S.Yu. *Kvantovaya Elektron.*, **38**, 1101 (2008) [*Quantum Electron.*, **38**, 1101 (2008)].
140. Pichugin S.Yu. *Kvantovaya Elektron.*, **38**, 736 (2008) [*Quantum Electron.*, **38**, 736 (2008)].
141. Tellinghuisen J., Phillips L.F. *J. Phys. Chem.*, **90**, 5108 (1986).
142. Komissarov A.V., Goncharov V., Heaven M.C. *Proc. SPIE Int. Soc. Opt. Eng.*, **4184**, 7 (2001).
143. Macler M, Nicolai J.P., Heaven M.C. *J. Chem. Phys.*, **91**, 674 (1989).
144. Waichman K., Rybalkin V., Katz A., Dahan Z., Barmashenko B.D., Rosenwaks S. *J. Appl. Phys.*, **102**, 013108 (2007).
145. David D. *Chem. Phys. Lett.*, **93**, 16 (1982).
146. Nota M., Bouvier A.J., Bacis R., Bouvier A., Crozet P., Churassy S., Koffend J.B. *J. Chem. Phys.*, **91**, 1938 (1989).
147. Brami-Rosilio I., Waichman K., Barmashenko B.D., Rosenwaks S. *Proc. SPIE Int. Soc. Opt. Eng.*, **7131**, 7131OD (2008).
148. Schmiedberger J., Fujii H. *Appl. Phys. Lett.*, **78**, 2649 (2001).
149. Shepelenko A.A., Mikheyev P.A., Kupryaev N.V., Voronov A.I. *Izv. Ross. Akad. Nauk, Ser. Fiz.*, **64**, 1259 (2000).
150. Ionin A.A., Kochetov I.V., Napartovich A.P., Yuryshev N.N. *J. Phys. D: Appl. Phys.*, **40**, R25 (2007).
151. Hill A.E. *Appl. Phys. Lett.*, **91**, 041116 (2007).
152. Carroll D.L., Benavides G.F., Zimmerman J.W., Woodard B.S., Palla A.D., Verdeyen J.T., Solomon W.C. *Proc. SPIE Int. Soc. Opt. Eng.*, **7131**, 71310B (2009).
153. Didyukov A.I., Krasnoshchekov Yu.I., Kulagin Yu.A., Morozov V.A., Reshetnyak S.A., Shelepin L.A. *Kvantovaya Elektron.*, **9**, 731 (1982) [*Sov. J. Quantum Electron.*, **12**, 451 (1982)].
154. Zolotarev V.A., Kryukov P.G., Podmar'kov Yu.P., Frolov M.P., Yuryshev N.N. *Kvantovaya Elektron.*, **16**, 1095 (1989) [*Sov. J. Quantum Electron.*, **19**, 709 (1989)].
155. Jones I.T.N., Wayne R.P. *Proc. Roy. Soc. Lond. A*, **321**, 409 (1971).
156. Felder P. *Chem. Phys.*, **155**, 435 (1991).
157. Atkinson R., Baulch D.L., Cox R.A., Crowley J.N., Hampson R.F., Hynes R.G., Jenkin M.E., Rossi M.J., Troe J. http://www.iupac-kinetic.ch.cam.ac.uk, 2006.

158. Azyazov V.N., Antonov I.O., Heaven M.C. *J. Phys. Chem. A*, **111**, 3010 (2007).
159. Kabir M.H., Azyazov V.N., Heaven M.C. *J. Phys. Chem. A*, **111**, 10062 (2007).
160. Payne W.A., Thorn R.P., Nesbitt F.L., Stief L.J. *J. Phys. Chem. A*, **102**, 6247 (1998).
161. Atkinson R., Baulch D.L., Cox R.A., Hampson R.F., Kerr J.A., Rossi M.J., Troe J. *J. Phys. Chem. Ref. Data*, **26**, 1329 (1997).
162. Vagin N.P., Zolotarev V.A., Kryukov P.G., Pazyuk V.S., Podmar'kov Yu.P., Frolov M.P., Yuryshev N.N. *Kvantovaya Elektron.*, **18**, 33 (1991) [*Sov. J. Quantum Electron.*, **21**, 28 (1991)].
163. Azyazov V.N., Kabir M.H., Heaven M.C. *Proc. SPIE Int. Soc. Opt. Eng.*, **6454**, 64540K (2007).
164. Kaufman F., Kelso J.R. *J. Chem. Phys.*, **46**, 4541 (1967).
165. Kurylo M.J., Braun W., Kaldor A., Freund S.M., Wayne R.P. *J. Photochem.*, **3**, 71 (1974).
166. Klopovskii K.S., Kovalev A.S., Lopaev D.V., Rakhimov A.T., Rakhimova T.V. *Fiz. Plazmy*, **18**, 1606 (1992).
167. Okabe H. *Photochemistry of Small Molecules* (New York: Wiley, 1978; Moscow: Mir, 1981).
168. Gonzales M., Valero R., Anglada J.M., Sayos R. *J. Chem. Phys.*, **115**, 7015 (2001).
169. Azyazov V.N., Kabir M.H., Antonov I.O., Heaven M.C. *J. Phys. Chem. A*, **111**, 6592 (2007).
170. Sun F., Glass G.P., Curl R.F. *Chem. Phys. Lett.*, **337**, 72 (2001).
171. Bloss W.J., Rowley D.M., Cox R.A., Jones R.L. *J. Phys. Chem. A*, **105**, 7840 (2001).
172. Vöhringer C.M., Badini R.G., Argüello G.A., Staricco E.H. *Ber. Bunsenges. Phys. Chem.*, **94**, 1387 (1990).
173. Tellinghuisen J. *J. Chem. Phys.*, **58**, 2821 (1973).
174. Han J., Komissarov A.V., Tinney S.P., Heaven M.C. *Proc. SPIE Int. Soc. Opt. Eng.*, **4971**, 45 (2003).
175. Oum K.W., Hancock G. *J. Phys. Chem. A*, **101**, 2634 (1997).
176. Hathorn F.G.M., Husain D. *Trans. Faraday Soc.*, **65**, 2678 (1969).
177. Lee S., Rawlins W.T., Davis S.J. *Chem. Phys. Lett.*, **469**, 68 (2009).
178. Wayne R.P. *J. Photochem.*, **25**, 49 (1984).